Article

Nano- and Micro-Tribological Investigations of Boundary Layers on Axial Bearing Washers Tested under WEC Critical Conditions

Florian Pape [ID]

Institute of Machine Design and Tribology (IMKT), Leibniz Universitaet Hannover, An der Universität 1, 30823 Garbsen, Germany; pape@imkt.uni-hannover.de; Tel.: +49-511-7611-3392

Abstract: The formation of boundary layers on bearing surfaces due to the operational conditions has a significant influence on bearing lifetimes and frictional properties. Zinc dialkyldithiophosphate is an anti-wear additive widely used in oil and grease formulations that forms beneficial surface boundary layers. Under certain circumstances, this additive can cause early bearing failure due to white etching cracks (WEC) formation. By influencing chemical reactions and diffusion processes, the boundary films are suspected to be a reason for the emergence of WECs. The properties of these layers under WEC critical and uncritical conditions are of interest. To gain knowledge of these layers, nano- and micro-tribological tests were performed. One possibility is to measure the hardness by nanoindentation and scratching on and into the layers by nano scratch tests. Another way is to perform local resolved micro-pin-on-disk tests. Additionally, ToF-SIMS (Time-of-Flight Secondary Ion Mass Spectrometry) was performed on the bearing surfaces to conclude the chemical compositions of the boundary layers. In the focus was, if the measured properties of the layers can be correlated to the bearing's early failures due to WEC, frictional properties of the whole system, and the wear on the surfaces.

Keywords: micro tribology; tribo-chemistry; mechanochemistry; boundary layers; micro pin-on-disk; nano scratch; ToF-SIMS

1. Introduction

The formation of white etching cracks (WEC) is the focus of current research. Under certain lubricants, early failure of bearings can occur, featuring subsurface cracks with white etching flanks. Up to date, mainly the subsurface zone has been investigated for a better understanding of the crack formation. Greco et al. correlated the WEC initiation with the cumulative frictional heat energy [1]. Subsurface cracks were generated and analyzed by X-ray tomography. It could be demonstrated that the cracks can evolve subsurface without connection to the bearing raceway surface [2]. By performing measurements of hydrogen, it could be proven that hydrogen-influenced embrittlement enhances crack formation [3]. Drivers for the occurrence of WEC are the oil additives ZDDP (Zinc dialkyldithiophosphate) and rust preventative over-based calcium sulphonates [4]. ZDDP is widely used as an antioxidant, corrosion inhibitor, and anti-wear additive in oil. Phorer also regards an electrical component as a driver for WEC formation that can be caused by triboelectric charging at boundary layers [5]. Subsurface WEC are mainly concentrated in zones prone to higher surface slip [6]. In addition to temperature, shear stresses influence the tribofilm formation on the surface [7]. The boundary layers formed due to ZDDP feature higher local frictional properties on the bearings' surface [8]. The film formation based on ZDDP is investigated by tribometer tests to conclude the reaction kinetics and surface roughnesses. In the field of mild wear investigation, the ZDDP film formation is also investigated in terms of molecular dynamics. Boundary layers can be generated in dependence on the test conditions. Such layers can even be generated by the oscillation of an AFM (atomic force

microscopy) tip along a lubricated flat silicon surface [9]. The film formation is referred to as the mechanochemical mechanism and depends on pressure, induced shear stresses, and temperature. As these boundary layers consist of translucent glassy polyphosphates combined with zinc, sulfur, and iron, light microscopic surface measurements to conclude the roughness do not work. To obtain information on the structure, AFM has to be performed, or the surface has to be covered by a thin sputtered gold film [10]. Under tribological load, boundary films are formed at room temperature [7,11]. Mosey et al. proposed a molecular dynamic model showing that the polyphosphate chains of the tribofilm are cross-linked due to high contact pressure [12]. The kinetics of ZDDP-based tribofilm formation, in terms of the formation of a sulfur-rich initial layer on the steel surface, was addressed by Dorgham [13]. It was shown by Zhang et al., based on ball-on-disk tests, that induced shear stress reduces the thermal activation barrier for ZDDP tribofilm formation [7]. Prior nanoindentational studies proved the hardness of ZDDP-based boundary layers from 6–7 GPa with a film indentation depth of 50–60 nm [14].

To gain deeper insight into the boundary films of bearings prone to WEC, investigations deploying nanoindentation, scanning probe microscopy, Time-of-Flight Secondary Ion Mass Spectrometry (ToF-SIMS), and micro pin-on-disk tests were performed on bearing washers after test bench measurements. While classic tribology deals with macroscopic structures, nano- and micro-tribology work on the atomic and microscopic scale. The effects on this scale have to be regarded for the investigation of sliding surfaces under the lowest loads. To analyze the friction of nano-contacts, work has been done in the field of hard disk drives. The contact of the slider to the hard disk with consecutive lifting at the start process and landing at the stop process is the focus of numerous studies [15–17]. For this purpose, systems with high resolution were developed, allowing to measure friction in test cycles. One approach is to use such a tester for micro-tribological investigations of bearing surfaces.

Lubrication has a large influence on the development of boundary layers in tribological contacts. Tohyama et al. presented that polymer additivated oil can reduce the frictional force in a block against the ring test [18]. Polymer films could be proven with ToF-SIMS measurements on the surface. A model of adsorbed polymers on metallic surfaces was introduced by Tohyama, as shown in Figure 1 [18].
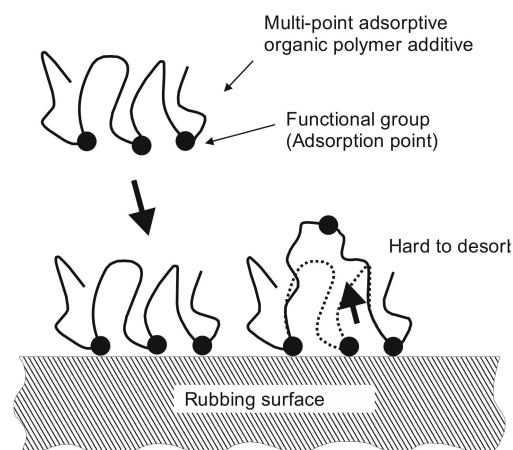

Figure 1. Model according to Tohyama et al. [18] of adsorbed polymers on metallic surfaces.

The correlation of chemical processes and surface layers for additivated greases was investigated by Wiendl et al. [19]. To analyze these layers, nanoindentational studies and ToF-SIMS measurements were performed on rolling bearings after life tests. It could be shown that antioxidants reduce the oxidation of the grease and have an influence on surface layers. The effects of polymer additivated greases on surface layers were analyzed by Gatzen et al. [20]. Rolling bearings were investigated by applying nanoindentational

tests and ToF-SIMS. The formation of surface layers could be shown, and effects on the surface roughness and hardness could be detected.

For the experiments in this study, axial bearings type 81212 were used on an FE8 laboratory-type test rig. Oil with ZDDP additives was used as a lubricant. Previous tests proved that bearings tested with the specific low additivated lubricant composition tend to early failure and WEC (White Etching Cracks). By varying the temperature or the axial load on the bearings, the influence on the bearing lifetime (early failure) and the development of boundary layers is of interest.

2. Materials and Methods

The experiment was performed in two steps. In the first step, cylindrical roller thrust bearings were subjected to life tests. Both the rollers and the disk (also called washer) materials are 100Cr6 (German standard corresponding to AISI 52100). The bearings were oil lubricated and tested under different operational conditions. After reaching the desired running time or an early bearing failure, the systems were disassembled, and in the second step of the experiment, the disks were subjected to nanoindentational tests, micro pin-on-disk tests, and ToF-SIMS. The axial bearings were cleaned before the surface analysis with n-hexan to remove all organic adhesives. Each of the axial bearings subjected to the life test was lubricated with a less additivated oil containing ZDDP additives and mounted in the FE-8 test rig. The oil was supplied at a constant flow rate of 0.1 L/min. Figure 2a represents the setup of the test rig. A tested axial bearing washer (after test with boundary layers) is shown in Figure 2b. The test is specified in the standard DIN 51819 for the mechanical–dynamic measurement of rolling contact bearing lubricants. The pre-load to the bearings was engaged with disk springs. To stabilize the bearing temperature, the test head was ventilated.
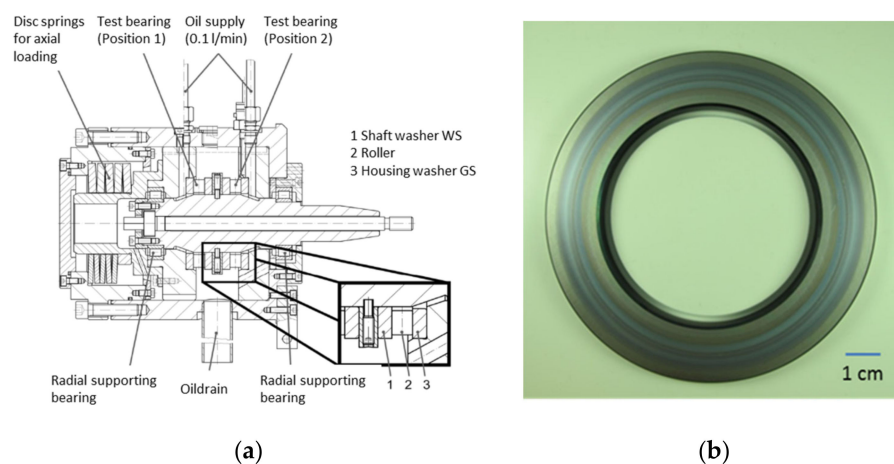

Figure 2. FE8 test rig for bearing life tests; (**a**) head of FE-8 test rig for characterization of rolling contact lubrication, (**b**) axial bearing washer with boundary layers after test.

The bearing life test consists of a run-in phase for 24 h at 500 rpm followed by a 176 h test run at 750 rpm. A bearing failure before reaching the desired total of 200 h running time was determined by vibrational measurements. During the tests, the frictional torque and temperature were measured. For the tests, the temperature and load were varied to achieve a change in the mechanochemical conditions on the bearing's surface. Thus, boundary layers of different properties should be generated. The test conditions for the axial bearing washers are shown in Table 1. For the bearing tested at 100 °C, the test duration was 50:12 h, as the test rig stopped due to a detected bearing failure. The average frictional torque was 8.5 Nm. For the bearing under a higher temperature of 120 °C, the test length was 200 h, and the average frictional torque was 6 Nm.

Table 1. Test conditions and results for axial bearing washers.

Axial Bearing Washer	Temperature (°C)	Axial Load (kN)	Test Length (h:min)	Average Frictional Torque (Nm)
3 (TB 60-80)	80	60	200:00	10
1 (TB 60-100)	100	60	50:12	8.5
2 (TB 60-120)	120	60	200:00	6
4 (TB 80-100)	100	80	37:52	13

With a reduced temperature of 80 °C, the test length was 200 h, and the average frictional torque reached a value of 10 Nm. In the case of the bearing with the increased load, the test failed earlier with 37:52 h, and the average frictional torque was 13 Nm. For the bearing TB 60-100, WEC could be proven on the rollers and the washer. Figure 3a depicts a cross-section with a WEC subsurface in the bearing washer. An ultrasonic image is shown in Figure 3b, proving subsurface cracks mainly in the outer high-slip zone of the bearing washer. Due to the bearing kinematics, a portion of up to ±10% slip is achieved on the inner and outer high slip zones.

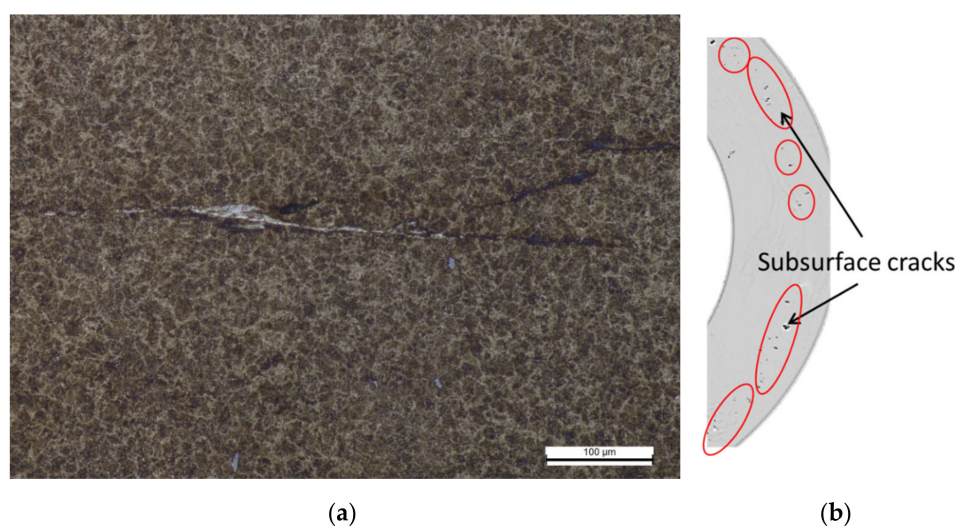(**a**)　　　　　　　　　　　　　　　　　　　(**b**)

Figure 3. Bearing washer TB 60-100, (**a**) Cross-section on bearing washer (TB 60-100) with subsurface WEC, (**b**) Ultrasonic image of subsurface cracks (TB 60-100).

To obtain the nanomechanical properties of the axial bearing washers, nanoindentational tests were performed. The tests were carried out using a Hysitron TriboIndenter® (Bruker Corporation, Billerica, MA, USA), allowing scanning probe microscopy. The test setup is based on a 3D transducer with a three-plate capacitor for vertical displacement and two three-plate capacitors for horizontal displacement. To measure the hardness, a triangular diamond Berkovich tip (tip radius of approx. 100 nm) is mounted on an elastically suspended pick-up electrode which is placed between the capacitors. The material behavior of the coating and the substrate is characterized by load-displacement curves. A load of 1 mN was applied to the tip. The hardness values were calculated with the unloading curve of the indentation tests applying the method of Oliver and Pharr [21]. For the hardness measurement, 12 indents were performed in 1 area, and the average value was calculated. The measurement itself was performed at specific points on the bearing washer, starting at the outside of the washer at a 1 mm distance to the outer rim. The surface properties were evaluated by single nano scratch tests. This allowed measuring the tribological behavior in point contact. The scratch tests were performed with a cono-spherical diamond tip (tip radius of 280 nm). The cono-spherical tip is moved along the substrate and scratches into the surface with increasing load. For the single scratch tests, the load force was increased continuously over the scratch length, reaching the final force. The final force was 1 mN. The effective scratch length was 9 µm. After the scratch, the surface

was mapped by scanning probe microscopy (SPM) to investigate the plastic deformation and pile-up beside the scratch. A scheme for a scratch test is shown in Figure 4. In a first step, the surface prior to the scratch is scanned under low load in a pre-scan. Afterward, the scratch is performed with increased load, and the tangential force is recorded (friction during plowing). After the scratch, a post-scan is performed on the scratch path, and the plastic deformation can be measured as shown in [22]. The procedure allows concluding the elastic and plastic properties of the surface as well as the frictional properties of the boundary layers under plowing.
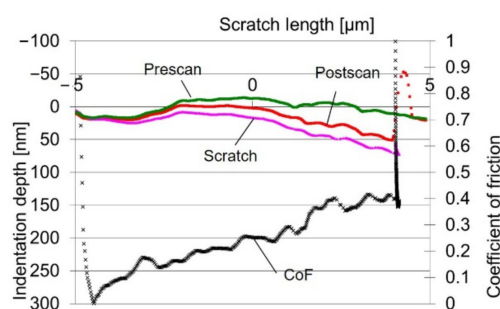

Figure 4. Scratch test on unused 100Cr6 bearing steel.

2.1. Micro Pin-on-Disk Tester

The tests were carried out with a micro pin-on-disk tester, which is based on a modified Center for Tribology (CETR, now Bruker, USA) Olympus HDI reliability spin-stand. The tester is depicted in Figure 5a. The test stand was originally developed to investigate the head-to-disk interface of a hard disk drive (HDD) [23]. This allows applying continuous start–stop (css) test cycles, a test commonly used for hard disk drive tests.
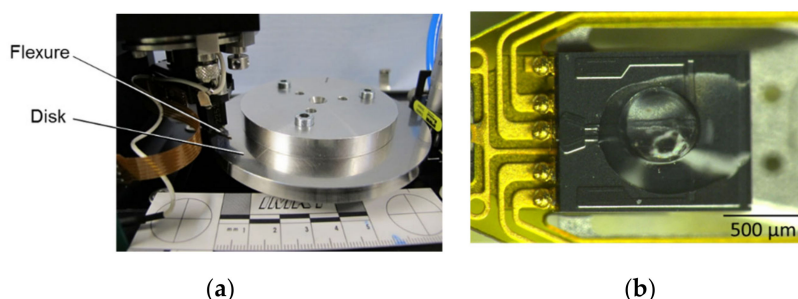

(**a**)   (**b**)

Figure 5. Micro pin-on-disk tester; (**a**) Setup of the micro-pin-on-disk test, (**b**) Sapphire half ball mounted on the flexure.

A sapphire half ball as a test specimen was attached with adhesive to the slider of an HDD recording head (head gimbal assembly—HGA) (Figure 5b). The diameter of the test specimens was 500 μm. Next, the slider was mounted on the tester's arm. The desired normal force of 30 mN was applied by a vertical displacement of the slider in the tester. The arm represents the stationary part of the micro-pin-on-disk tester while the disk is rotating. The frictional force during sliding was measured by strain gauges integrated into the tester's head when the slider was in contact with the rotating disk. As a counterpart, a 95 mm diameter axial bearing disk (also called a washer) was used. During the test cycles, the coefficient of friction was recorded. By measurement of consecutive test cycles, not only the friction during a test but also the development of the friction over the test cycles at the starting and stopping points can be analyzed. To investigate the raceway on the bearing washers, the test specimen was set on different circumferences in defined positions. The steel disk was rotated for the tests at 1 rpm. For the conducted tests, the tester ran for five revolutions for each test cycle with a start and stop procedure. For the whole test, the procedure was repeated 10 times.

2.2. Time-of-Flight Secondary Ion Mass Spectrometry

The chemical compositions of loaded and unloaded areas on the washer surfaces were determined at the Physikalisches Institut, Westfälische Wilhelms-Universität Münster, using a ToF-SIMS instrument comparable to the ToF-SIMS IV of IONTOF GmbH, Germany. It is equipped with a bismuth liquid metal ion gun for high-resolution imaging and a noble-gas electron-impact ion gun for sputter erosion in dual beam depth-profile analysis.

Time-of-Flight Secondary Ion Mass Spectrometry (ToF-SIMS) is a surface analytical method for determining the atomic and molecular composition of surfaces of solid-state materials. Using this method, the surface of a solid-state target is bombarded with energetic primary ions causing the sputtering of the outermost monolayers of the target. Amongst the emitted particles, positively or negatively charged atoms or molecules, the so-called secondary ions, can directly be analyzed according to their mass-to-charge ratio determined via mass spectrometer [24–26].

The special merits of ToF-SIMS are a high detection probability combined with high surface sensitivity. The main focus of applications is on trace element analysis, the determination of lateral distributions of atoms and molecules on the surface, and the analysis of the composition of boundary layers using depth profiling. Due to this, ToF-SIMS is ideally suited for the analysis of tribologically built-up boundary layers, including the adsorptive layer formed from oil additive components, and to advance the understanding of the interaction of all materials involved [27–31].

3. Results

3.1. Nanoindentational Test Results

The first group of bearing washers (TB 60-100) were tested under the test conditions typically used for mechanical–dynamic measurement of rolling contact bearing lubricants (100 °C, 60 kN load). For the following tests, one bearing washer of the group was chosen as representative. After the macroscopic test, the hardness of the bearing's surface was measured by nanoindentation. The surface is depicted in Figure 6. The color of the raceways changed significantly. The hardness on the surface measured along the surface starting at the outer rim of the bearing washer is shown in Figure 7.
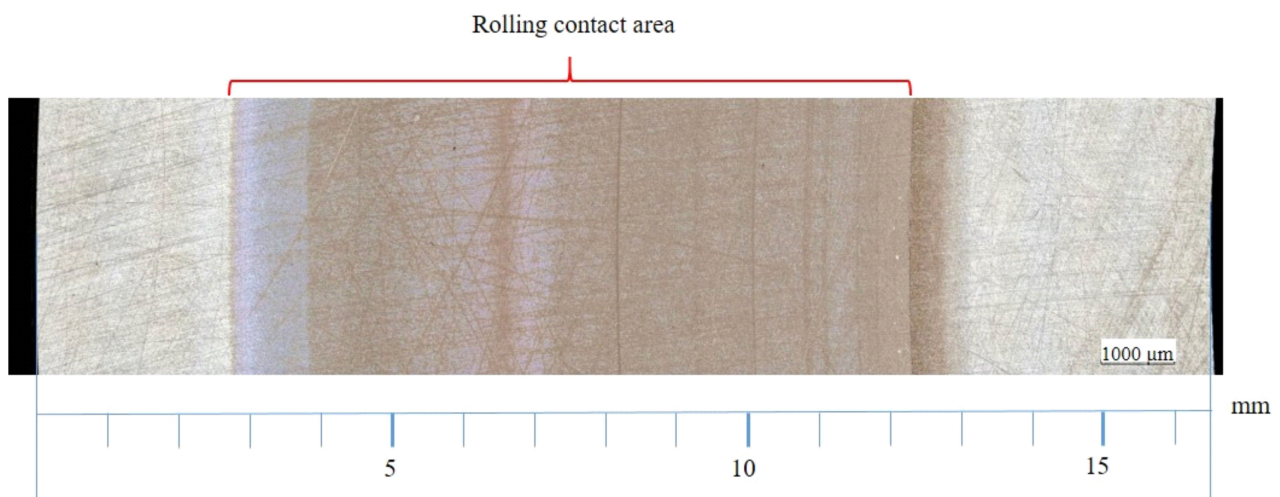

Figure 6. Photograph of the surface of bearing washer TB 60-100 (processed at a load of 60 kN and a temperature of 100 °C).
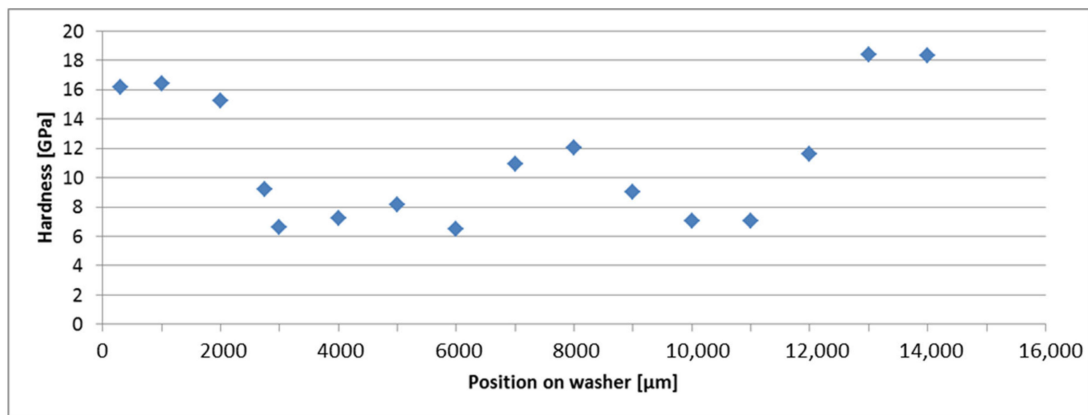
Figure 7. Hardness measurement on the surface of the bearing washer TB 60-100 (100 °C, 60 kN load).

In the area where the raceway is visible, the hardness is reduced. In the middle of the raceway, where pure rolling of the rolling bearing elements occurred, the hardness increases slightly but remains lower than outside the raceway.

In addition to the hardness measurement, nano scratch tests were performed on the surface. Figure 8 depicts exemplary SPM mages of scratches in specific positions. Outside the raceway, at 1000 µm from the outer rim of the washer (Figure 8a), the scratch is shallow with little material pile-up. The original surface topography remains on the surface. On the raceway at 3000 µm (Figure 8b), the scratch is wider and more pile-up can be found beside the scratch. The surface topography is flattened, while a superimposed surface roughness can be found. On the position 8000 µm, the scratch is clearly visible, showing some pile-up (Figure 8c). On the surface, a fine roughness can be found. The measurement on position 11,000 µm (Figure 8d) shows a comparable scratch on the surface with a similar roughness as on the position at 8000 µm.
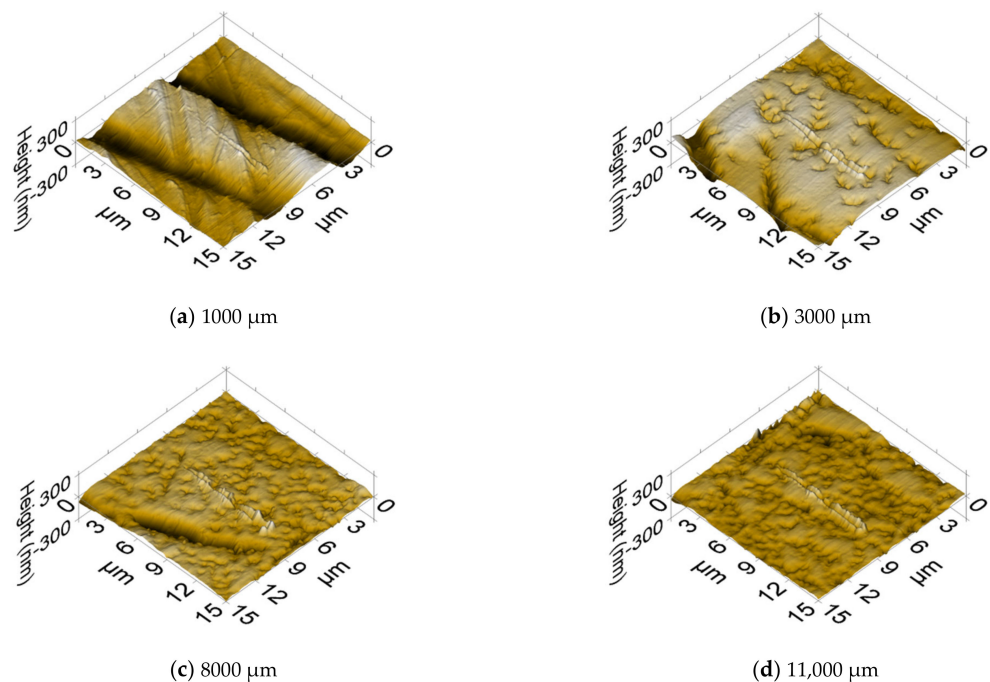

(**a**) 1000 µm

(**b**) 3000 µm

(**c**) 8000 µm

(**d**) 11,000 µm

Figure 8. Scanning probe microscopy (SPM) images for scratch tests at specific regions on bearing washer TB 60-100; (**a**) unloaded area at 1000 µm, (**b**) on the raceway at 3000 µm, (**c**) on the raceway at 8000 µm, (**d**) on the raceway at 11,000 µm.

An exemplary scratch test is shown in Figure 9. The surface structure of the tribofilm can be seen clearly. The plastic deformation of the tribofilm due to the scratch can be visualized. The tribofilm features less elastic and more plastic deformation while plowing the scratch tip through the tribofilm.
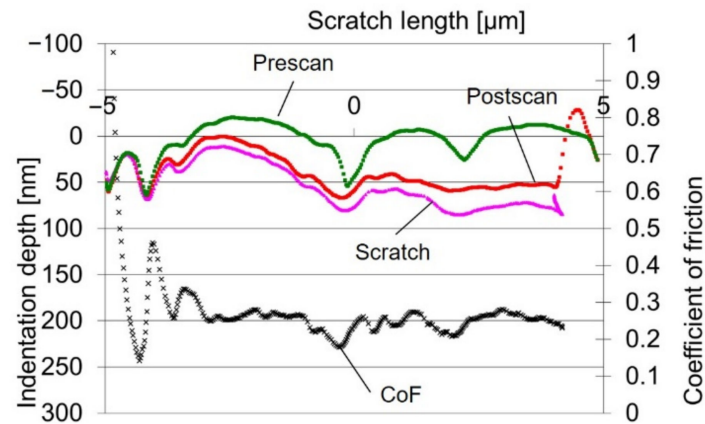

Figure 9. Scratch tests on TB 60-100—Position 3000 μm.

Based on Scanning probe microscopy (SPM) images of the nanoindentational measurements, the Root Mean Square (RMS) roughness R_q was calculated. The R_q values for the position on the bearing washer are shown in Figure 10. The roughness on the outer and inner slip zones is significantly reduced. In the zone where pure rolling of the rolling bearing elements occurred, the roughness is less reduced compared to the roughness outside the rolling contact area.
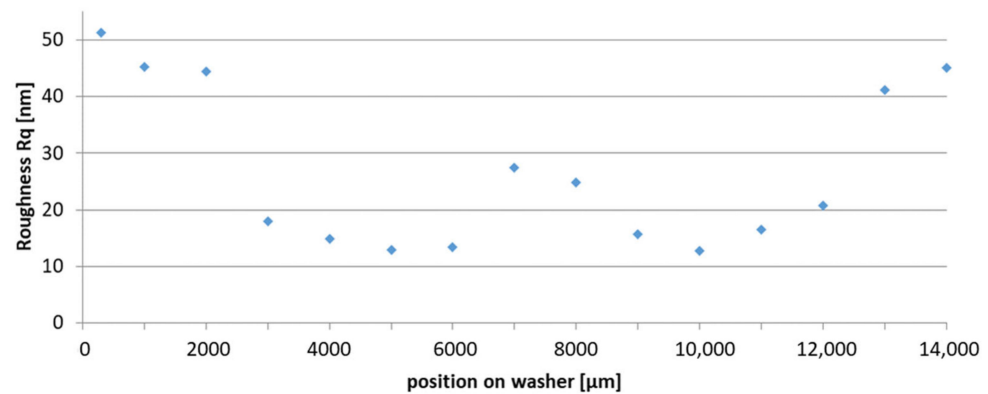

Figure 10. Root Mean Square (RMS) roughness R_q of the bearing washer TB 60-100 (100 °C, 60 kN load) based on SPM.

The second group of bearing washers TB 60-120 were tested under increased temperature (120 °C, 60 kN load). For the micromechanical tests, one bearing washer of this group was chosen as representative. For the bearing washer, the surface is shown in Figure 11. The color of the raceway shows different regions of more or less blue color. Additionally, an image of scars caused by slipping wear is depicted in Figure 12a. A detailed SPM image of a single scar is shown in Figure 12b; the width of the scar is approx. 100 microns, the length is 20 microns, while the depth is in the range of 50 nm.
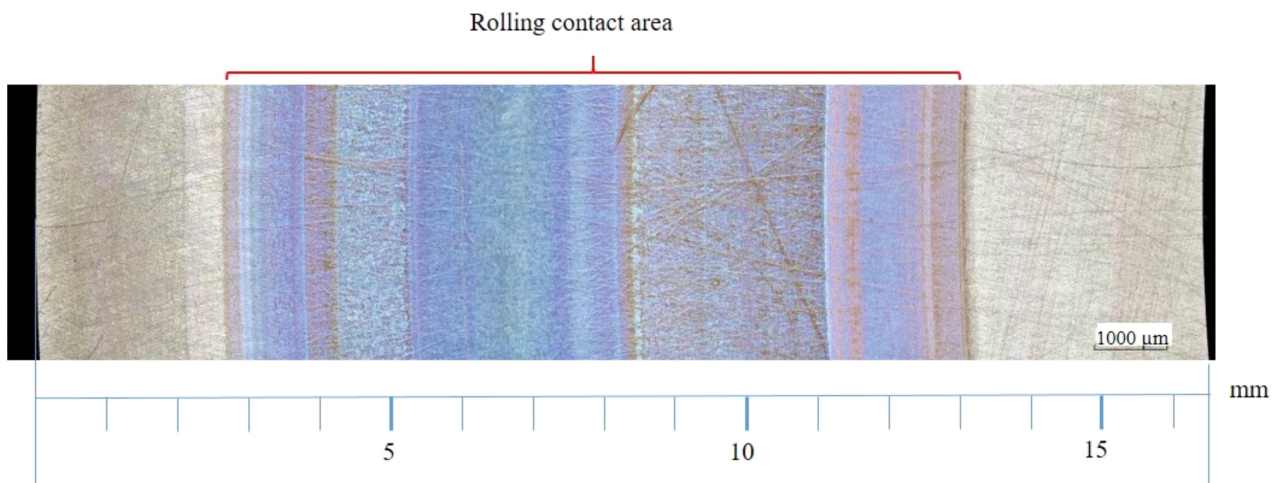
Figure 11. Photograph of the surface for the bearing washer TB 60-120 (60 kN load, 120 °C).
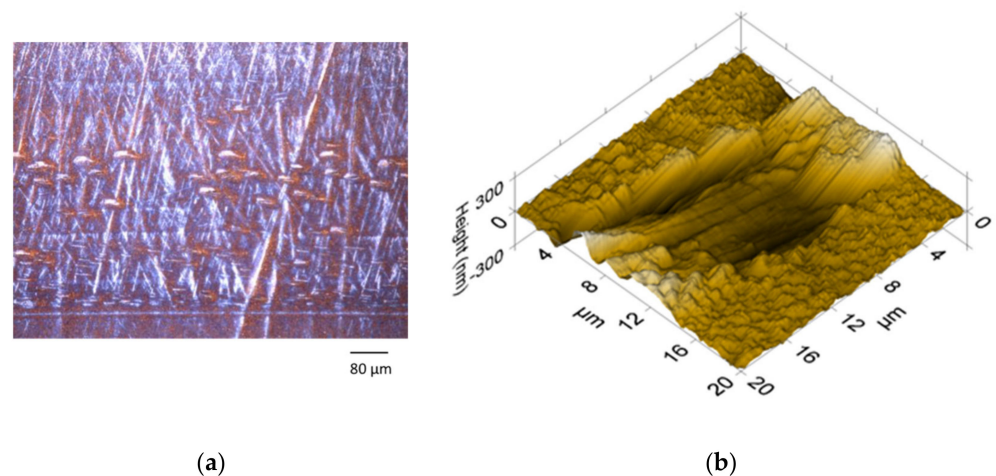

(**a**)   (**b**)

Figure 12. Slipping wear on position 3300 μm; (**a**) photograph, (**b**) scanning probe microscopy (SPM) image.

The hardness of the surface is shown in Figure 13. In the area where the raceway is visible, the hardness is reduced. On some tracks, a drastically reduced hardness can be found. In the middle of the raceway, where pure rolling of the rolling bearing elements occurred, the hardness increases only on one position (measured on 8300 μm) slightly but is lower than outside the raceway.

Figure 14 depicts exemplary SPM images of the scratches at specific positions on the raceway. Outside the raceway at 300 μm (Figure 14a), the scratch is shallow. The original surface topography can be found on the surface. On the raceway at 3300 μm (Figure 14b), the scratch is performed in a slipping wear scar. The scratch is shallow and little pile-up can be found beside the scratch. The surface topography is flattened beside the wear scar, and a superimposed roughness can be found. At the position of 8000 μm, the scratch is visible, and a fine surface roughness can be found on the surface (Figure 14c). A scratch test directly beside the previous one on 8300 μm was conducted (Figure 14d). In this position, the hardness is increased. The scratch is clearly visible with some pile-up. The roughness is reduced while the surface is flattened. The roughness values are shown in Figure 15. The roughness of the rolling contact zone is reduced. While the RMS roughness at the outer and inner slip zones is reduced to values down to 10 nm, in the middle of the contact zone (where pure rolling occurs), the roughness features values of 20 nm.
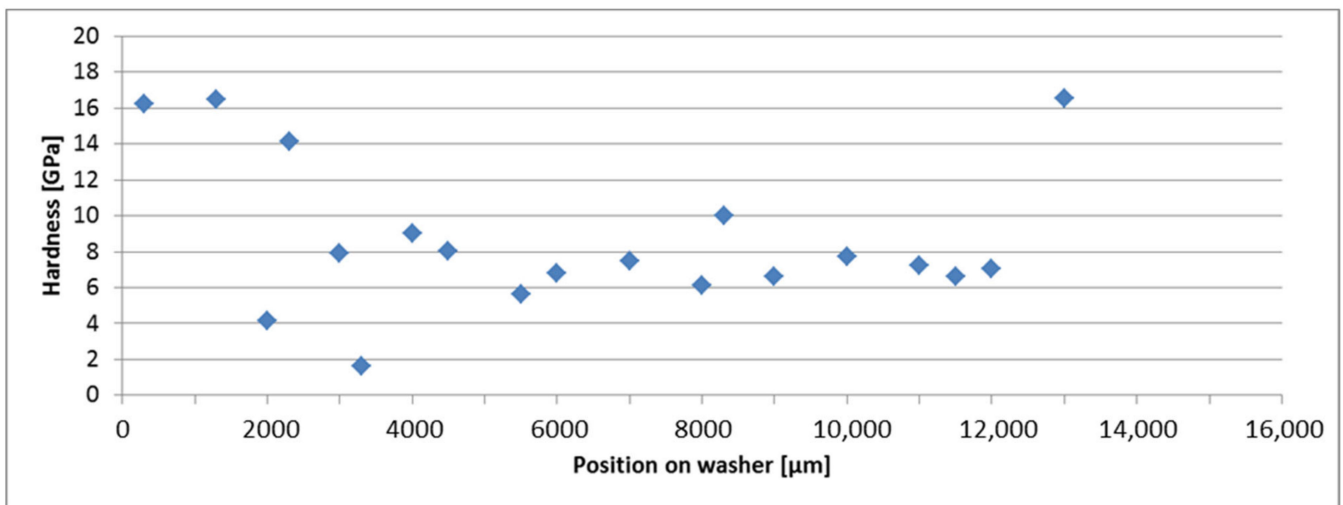
Figure 13. Hardness measurement on the surface for the bearing washer TB 60-120 (60 kN load, 120 °C).
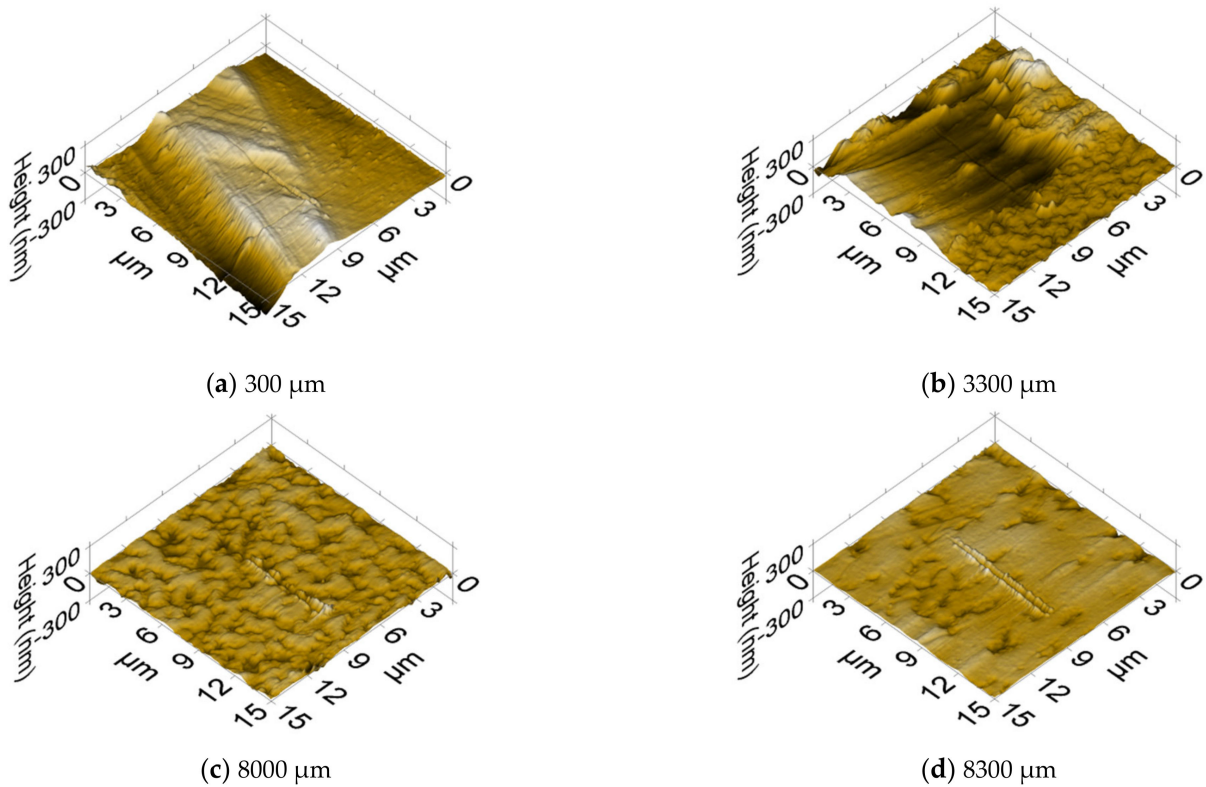

(**a**) 300 μm

(**b**) 3300 μm

(**c**) 8000 μm

(**d**) 8300 μm

Figure 14. Scanning probe microscopy (SPM) images for scratch tests at specific regions on the bearing washer TB 60-120; (**a**) unloaded area at 300 μm, (**b**) on the raceway at 3300 μm, (**c**) on the raceway at 8000 μm, (**d**) on the raceway at 8300 μm.
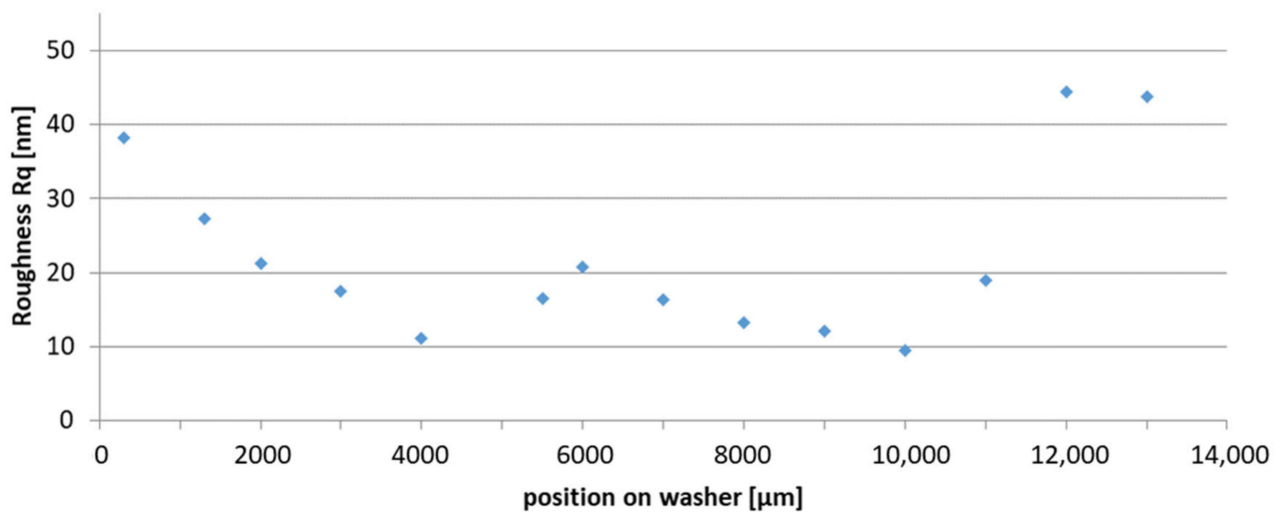
Figure 15. Root Mean Square (RMS) roughness Rq of the bearing washer TB 60-120 (120 °C, 60 kN load) based on SPM.

The third group of bearing washers TB 60-80 were tested under reduced temperature (80 °C, 60 kN load). For the tests, one bearing washer of the group was chosen as representative. The surface for the third bearing washer is depicted in Figure 16.
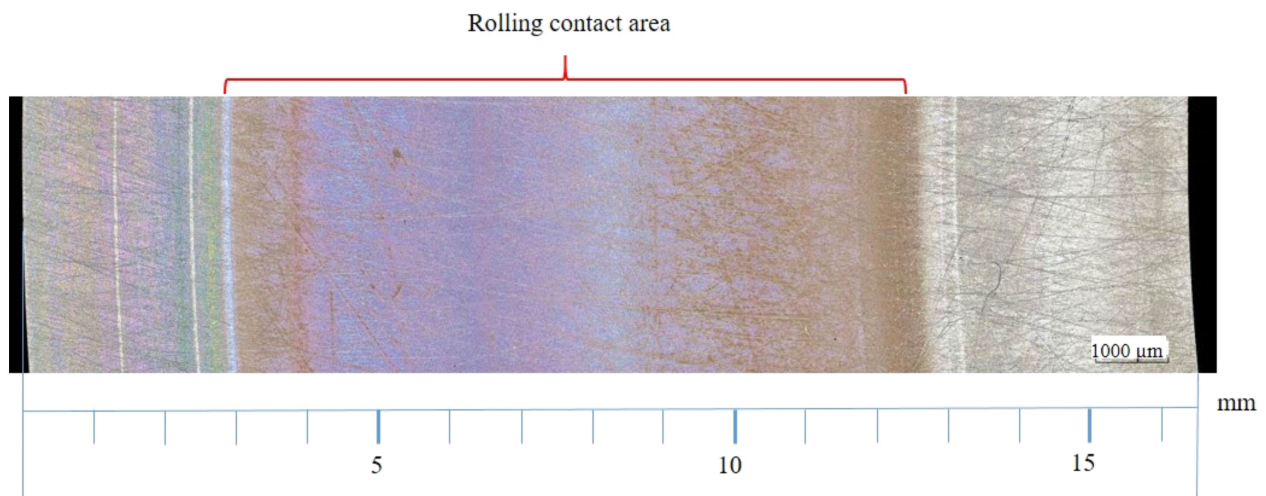

Figure 16. Photograph of the surface for a bearing washer TB 60-80 (60 kN load, 80 °C).

For this bearing, the raceway is clearly visible; on the outer side, the surface shows a significant change in color. Figure 17 shows the hardness of the surface. In the outer region of the raceway (at 1200 μm), the hardness is partly increased, on the inner region of the bearing outside the raceway, the hardness shows higher values (at 14,000 and 15,000 μm). Directly at the outer region (at 1000, 1500, and 2000 μm) of the bearing, the hardness is drastically reduced; on the raceway, the hardness is on a comparable level to the second bearings raceway with approx. 8 GPa. The nano scratch tests show that even on the outer bearing zone, the surface features a very soft boundary layer. SPM images for the third bearing washer are depicted in Figure 18.
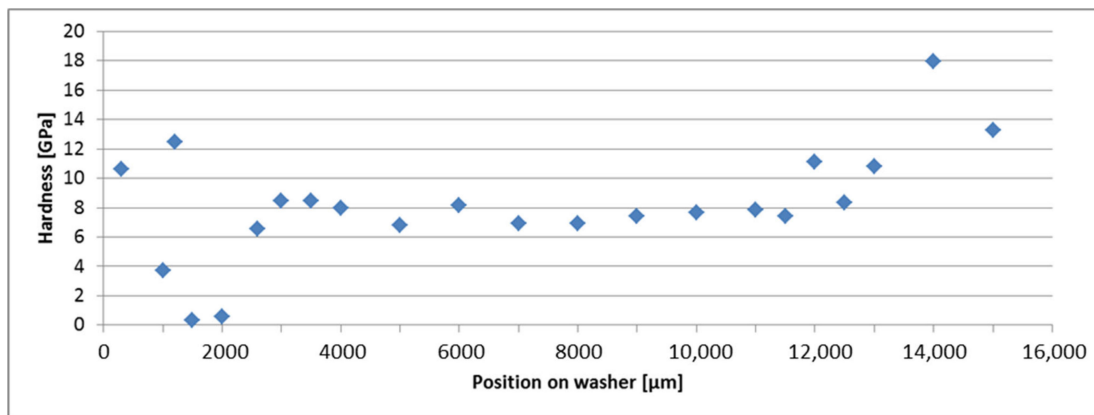
Figure 17. Hardness measurement on the surface for the third bearing washer (80 °C, 60 kN load).
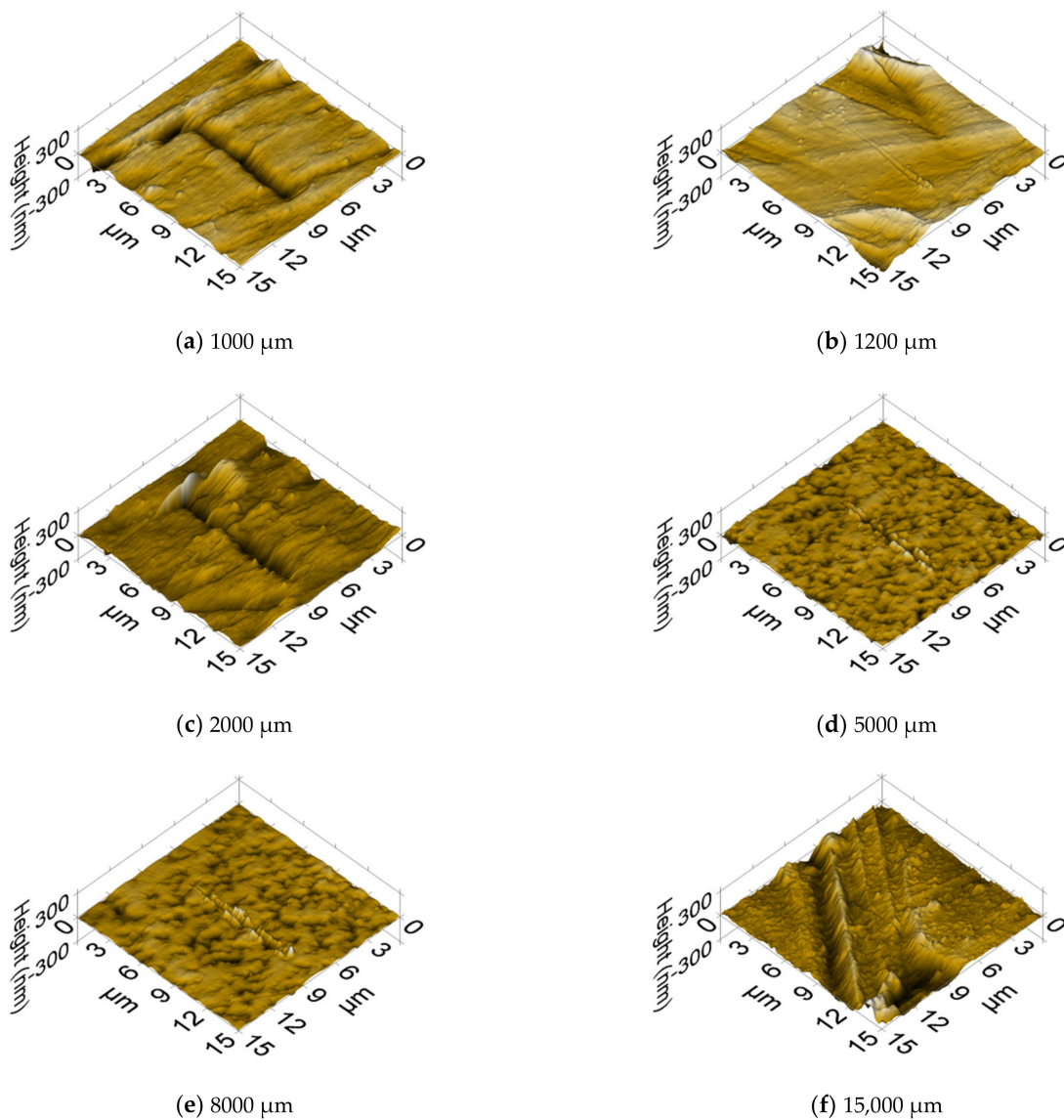

(**a**) 1000 μm

(**b**) 1200 μm

(**c**) 2000 μm

(**d**) 5000 μm

(**e**) 8000 μm

(**f**) 15,000 μm

Figure 18. Scanning probe microscopy (SPM) images for scratch tests of specific regions on the bearing washer TB 60-80; (**a**) on the raceway at 1000 μm, (**b**) on the raceway at 1200 μm, (**c**) on the raceway at 2000 μm, (**d**) on the raceway at 5000 μm, (**e**) on the raceway on 8000 μm, (**f**) unloaded area on 15,000 μm.

At the position of 1000 µm, the indent shows a deep scratch on the surface (Figure 18a). The bearing's surface is smooth. Beside this position, there is a circumference track at 1200 µm featuring higher hardness (Figure 18b). The scratch in this area is shallow. The surface itself shows a topography with higher roughness, like in the unloaded area. At the position of 2000 µm, the scratch is deep and very wide (Figure 18c). On the raceway at the positions 5000 µm (Figure 18d) and 8000 µm (Figure 18e), the scratch tests resulted in shallow scratches with some pile-up. The topography on the surface is smooth with a superimposed roughness. The surface on the raceway between 3000 µm and 11,000 µm features a similar topography with a fine superimposed roughness. In the unloaded area outside the raceway at 15,000 µm, the scratch is shallow with little pile-up (Figure 18f). The surface topography features a high roughness like an unused bearing. For comparison, the roughness of the bearing washer is shown in Figure 19. On the contact zone, the roughness features values between 10 and 20 nm. At the outer diameter of the bearing, a reduced RMS roughness is measured, which can be caused by a surface film due to thermal film formation.
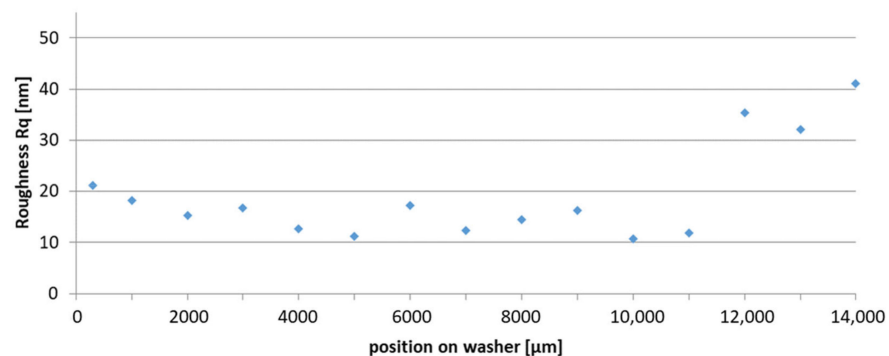

Figure 19. Root Mean Square (RMS) roughness Rq of the bearing washer TB 60-80 (80 °C, 60 kN load) based on SPM.

The higher load of 80 kN was applied to the fourth group of bearing washers TB 80-100 (80 kN load, 100 °C). In this case, for the following tests, one bearing washer of the group was chosen as representative. The surface of the fourth bearing washer is depicted in Figure 20. The raceway on the surface is clearly visible; on the outer side, it shows a more uniform color compared to the inner side of the raceway with a border in the middle of the bearing. Especially on the inner side, scars and pittings can be found due to wear. The hardness of the surface is shown in Figure 21. Besides the raceway, the hardness features high values up to 20 GPa. On the raceway, the hardness is decreased with values of approx. 10 GPa. Compared to the other bearings, these values are increased for the raceways.
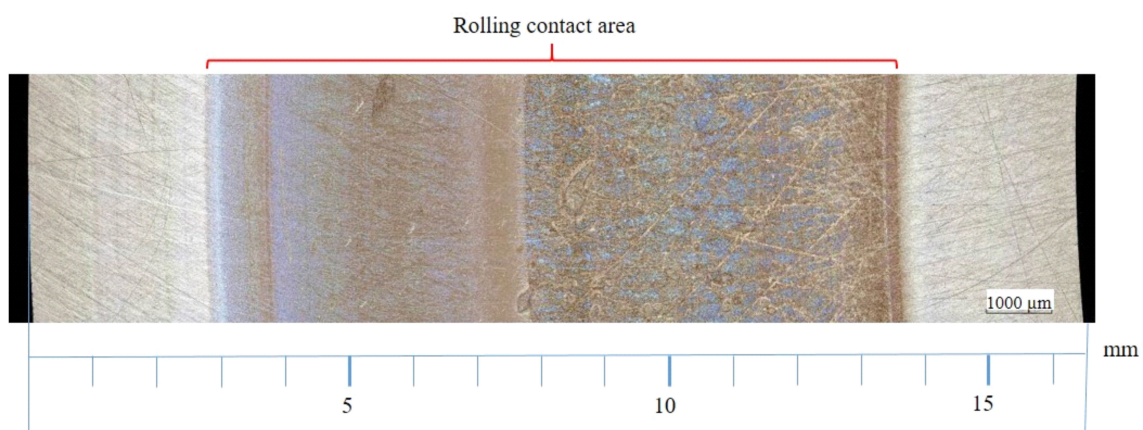

Figure 20. Photograph of the surface for the bearing washer TB 80-100 (80 kN load, 100 °C).
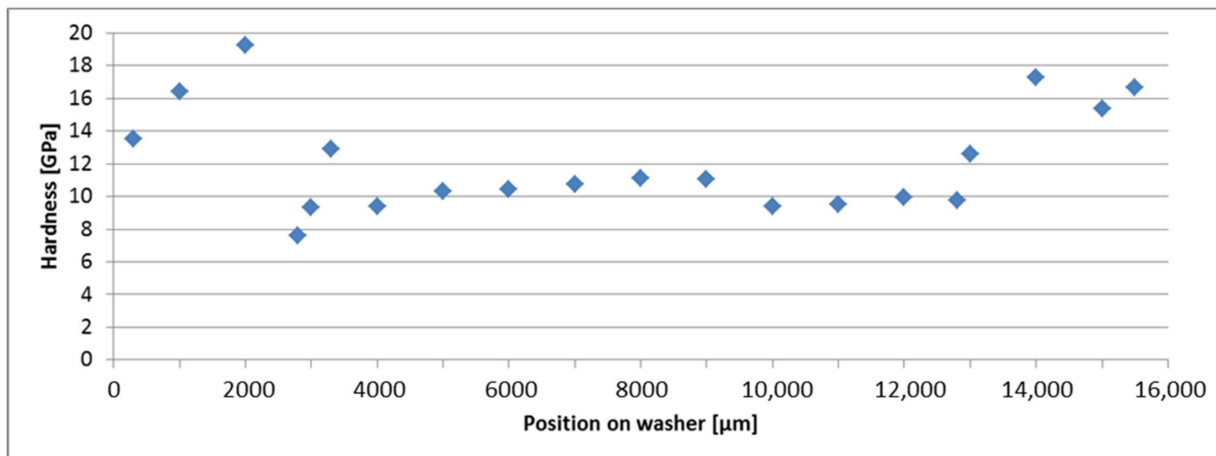
Figure 21. Hardness measurement on the surface for the bearing washer TB 80-100 (80 kN load, 100 °C).

The SPM images for the exemplary scratch tests are shown in Figure 22. For the position at 1000 μm, the scratch is shallow (Figure 22a).
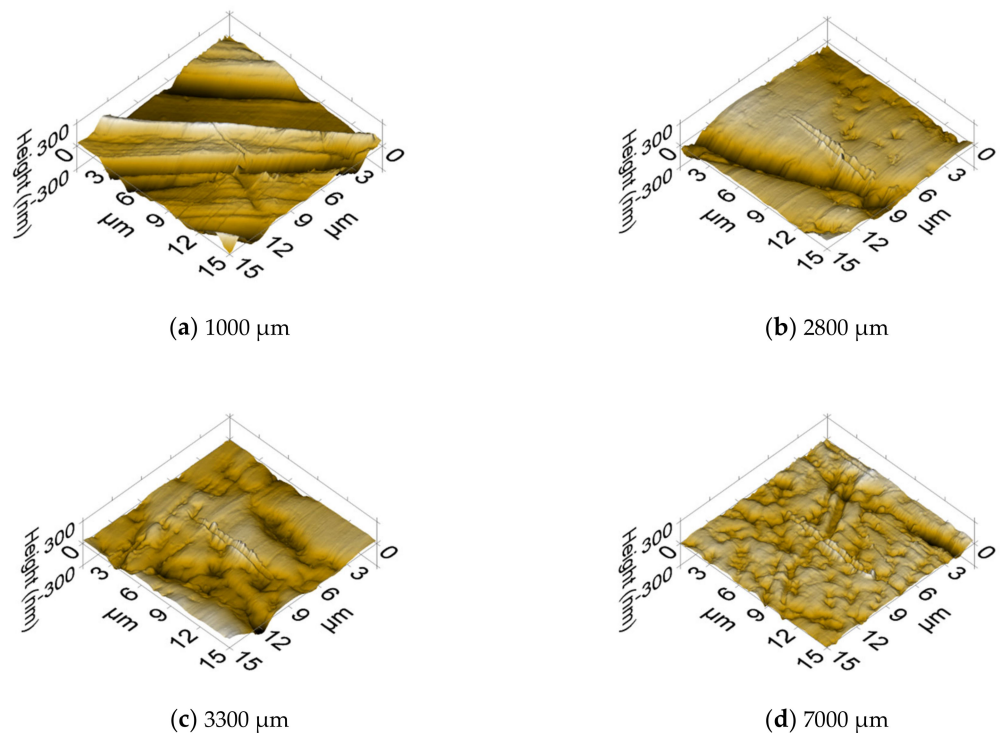

(**a**) 1000 μm

(**b**) 2800 μm

(**c**) 3300 μm

(**d**) 7000 μm

Figure 22. Scanning probe microscopy (SPM) images for scratch tests of specific regions on the bearing washer TB 80-100; (**a**) unloaded area at 1000 μm, (**b**) on the raceway at 2800 μm, (**c**) on the raceway at 3300 μm, (**d**) on the raceway at 7000 μm.

The surface topography features tool marks. For the position 2800 μm, the scratch is shallow and shows some pile-up, while the surface is flattened and shows little superimposed roughness (Figure 22b). The scratch on the position 3300 μm (Figure 22c) is shallow and features pile-up. The superimposed roughness is increased. For the position 7000 μm, the scratch remains shallow with some pile-up (Figure 22d). The surface is smoothened with a superimposed roughness. The roughness of the bearing washer is shown in Figure 23. The roughness is reduced with values around 20 nm on the rolling contact zone. Only at

the inner high slip zone, the RMS roughness features values of 10 nm. On average, the roughness is higher on the rolling contact zone than for the bearings run at a lower load.
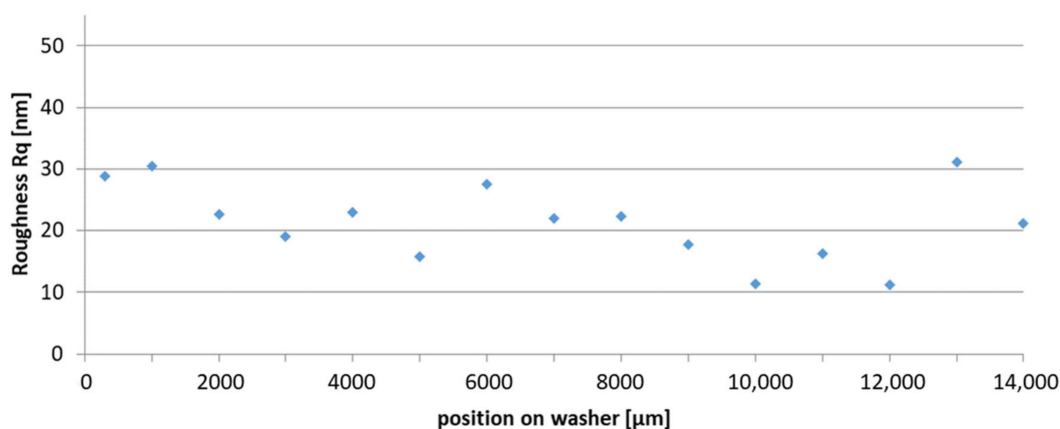

Figure 23. Root Mean Square (RMS) roughness Rq of the bearing washer TB 80-100 (100 °C, 80 kN load) based on SPM.

3.2. Micro Pin-on-Disk Test Results

For the bearing washer TB 60-100 (tested under 60 kN load, 100 °C), the CoF (coefficient of friction) was measured on the surface by applying the micro pin-on-disk tester with a sapphire half ball as a test specimen. Figure 24 shows the CoF for this bearing for different positions on the circumference of the bearing washer. The CoF (coefficient of friction) was measured on specific circumferences to investigate the behavior of the different areas on the raceways. For the first and the tenth cycle (each test cycle consists of 5 revolutions with a start and stop procedure), the CoF (which was calculated for the first 22 ms of each cycle) is depicted for the bearings. Thus, it is possible to conclude changes in the CoF through longer tests. To see an effect, the first and last cycles are depicted.
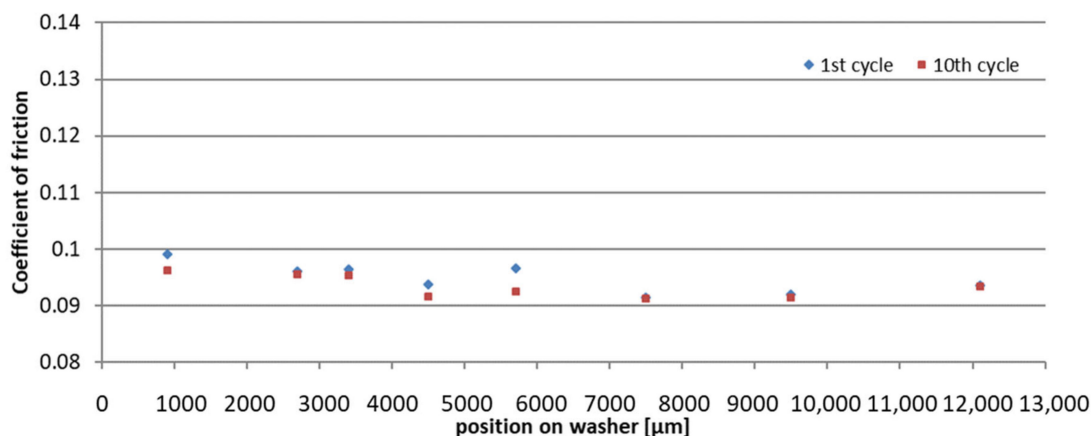

Figure 24. Coefficient of friction on the surface for the bearing washer TB 60-100 (60 kN load, 100 °C).

The CoF varies between 0.09 and 0.1, while the values on the outer side of the bearing are slightly higher. On the inner side of the bearing, the values are slightly lower and show no difference between the first and the last run.

The CoF for different positions on the circumference of the bearing washer TB 60-120 (tested under 60 kN load, 120 °C) is shown in Figure 25. The CoF varies between 0.09 and 0.15. On the raceway, the measurement of the CoF for the first and tenth test cycles on positions 3500 μm and 7700 μm changes significantly compared to the other measurement position. The CoF decreases from the first to the last test cycle. Compared to the other bearings, the variance of the CoF is increased.
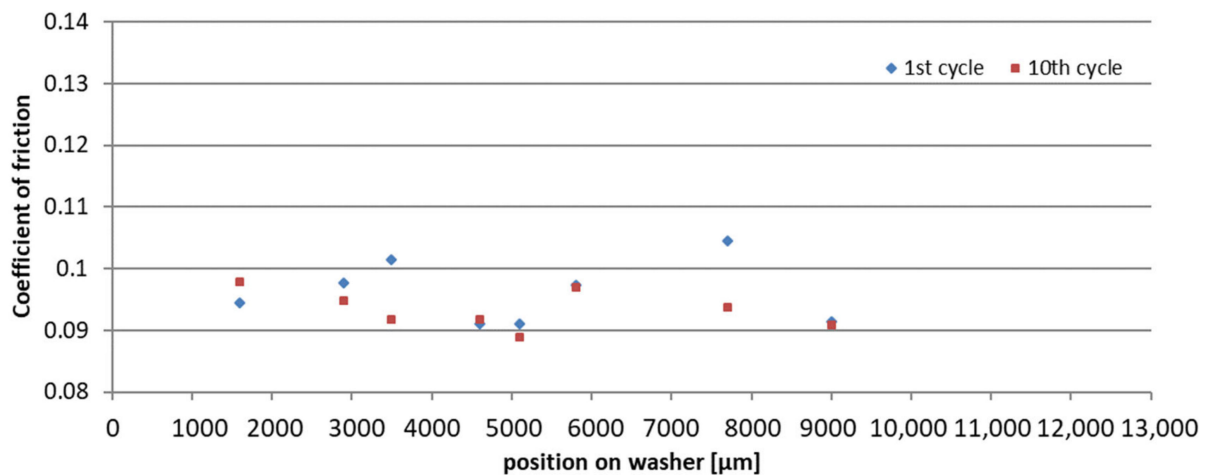
Figure 25. Coefficient of friction on the surface for the bearing washer TB 60-120 (60 kN load, 120 °C).

The CoF for different positions on the circumference of the bearing washer TB 60-80 (60 kN load, 80 °C) is depicted in Figure 26. The CoF varies between 0.09 and 0.13. On the outer zone of the bearing, the CoF is increased, and there is a major difference between the first and tenth test cycles. On the raceway itself, the CoF is lower with values between 0.09 and 0.1; between the test cycles, only minimal differences can be found.
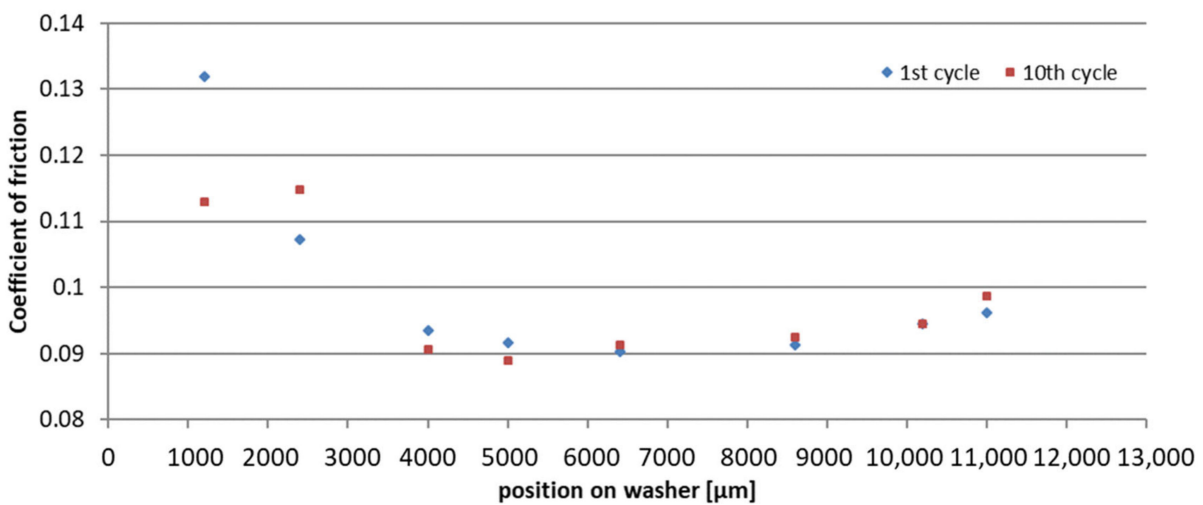

Figure 26. Coefficient of friction on the surface for the bearing washer TB 60-80 (60 kN load, 80 °C).

In the case of the bearing washer TB 80-100 (tested under a higher axial load of 80 kN and 100 °C), the CoF for different positions on the circumference is depicted in Figure 27. The CoF varies between 0.085 and 0.1. On the outer zone of the bearing, the CoF is slightly increased, and the first test cycle features generally higher values. On the inner side of the raceway, the CoF for the first test cycle is generally slightly lower than the tenth test cycle. For this bearing, the lowest CoF could be obtained.
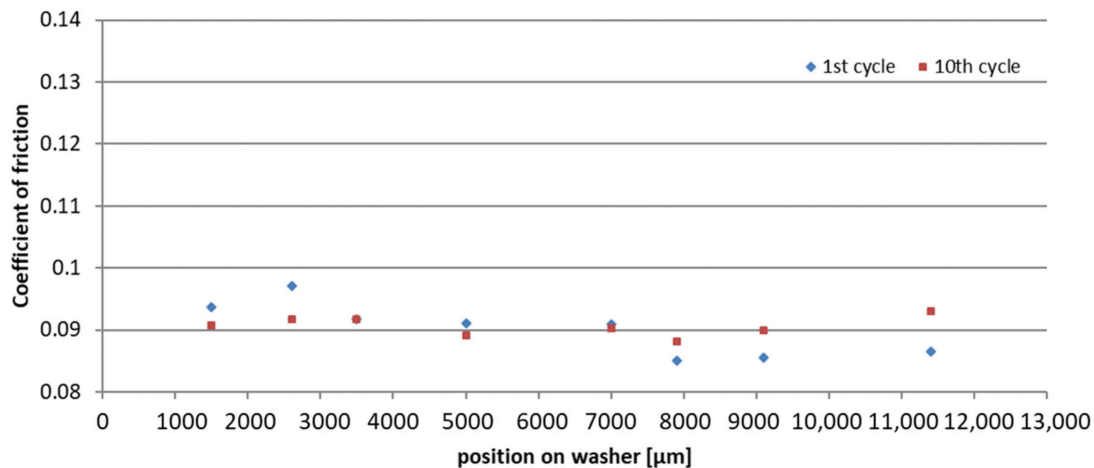
Figure 27. Coefficient of friction on the surface for the bearing washer TB 80-100 (80 kN load, 100 °C).

3.3. Time-of-Flight Secondary Ion Mass Spectrometry Results

In preparation for ToF-SIMS-analysis, the bearing washers were cut into four pieces. Prior to the analysis, the segments were cleaned in an ultrasonic bath (3 × 5 min) using n-hexane (SupraSolv) to remove the adhering oil film and expose the adsorbate layer.

On each washer, the lateral distribution of atoms and molecules on the surface was determined by applying the large area mapping mode of operation on an area of 14.7 mm × 1.8 mm, covering the whole rolling contact area, including adjacent areas outside the raceway. In order to avoid exceeding the static limit, two large area maps were recorded analyzing positively as well as negatively charged ions.

Figure 28 shows the distribution of selected positive (top) and negative (bottom) secondary ions obtained from a large area mapping of the washer surface of the test bearings TB 60-80 (left), TB 60-100 (middle), and TB 60-120 (right). The position of the raceway is marked in dark grey; however, the relative position depends on the backlash of the rolling elements in the cage, which is about ±250 μm. The light grey background marks the whole area of 15.8 mm of the polished washer surface. The outer rim of the washer is indicated by the position 0 mm. Every single image is normalized to itself, and bright areas depict high secondary ion intensities.

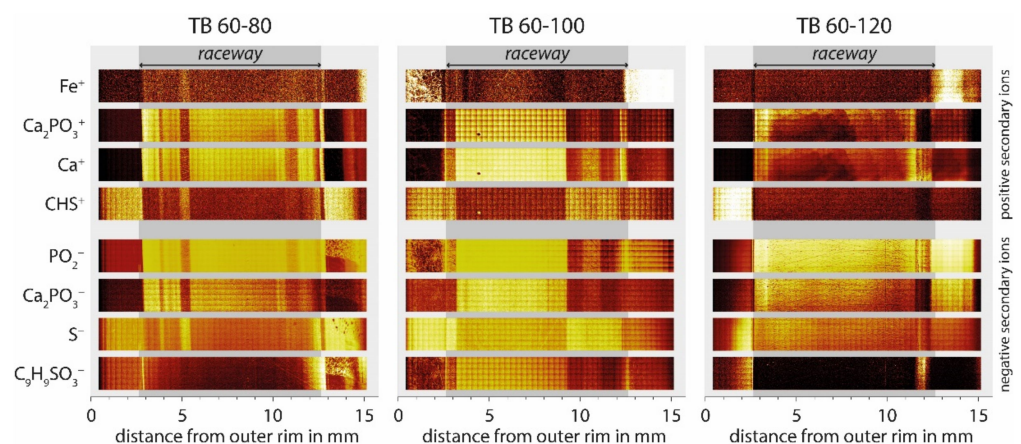**Figure 28.** Distribution of selected positive (top) and negative (bottom) secondary ions obtained from large area mappings of the washer surfaces of test bearings TB 60-80 (left), TB 60-100 (middle), and TB 60-120 (right).

As can be seen for TB 60-80 (left) and TB 60-100 (middle), several secondary ion signals show inhomogeneous distributions with clearly separated areas inside the raceway. With

TB 60-120 (right), all negative secondary ions show a much more uniform distribution inside the rolling contact area apart from areas near both edges of the rolling contact area. Note that large area maps of negative and positive secondary ions were obtained from different sites separated by a distance of about 2 mm. In the case of TB 60-120, the positive secondary ions were registered at a place where surface contamination, possibly zinc-containing, seems to cover parts of the raceway.

The occurrence of PO_2^-, $Ca_2PO_3^-$, $Ca_2PO_3^+$, and other molecules containing compounds of type P_xO_y ($x \geq 2$, $y \geq 3$; not shown) often indicate the formation of a phosphate glass layer [18,19]. With TB 60-80 and TB 60-100, those signals are mainly located within the raceway. With TB 60-120, those signals also show relatively high intensities outside the raceway, mainly in the inside region of the washer. This might be an indication of a pure thermally caused formation of a phosphate glass layer from ZDDP, according to Fujita [20]. He showed that with oil temperatures exceeding 80 °C, layer formation is not negligible and increases with increasing temperature and immersion time.

Another peculiarity can be seen comparing the secondary ion signal intensities obtained from different areas of the raceway. With all washers, but especially those from TB 60-80 and 60-100, differences in the secondary ion emission between high slip zones outside and inside the raceway are visible. This might indicate different conditions for molecule adsorption and film formation on the outer side of the raceway compared to those on the inner side. A reason might be found in different surface temperatures, probably induced by different kinds of slip, which can lead either to different chemical reactivity or to the deterioration of adsorbed molecules.

In addition, with TB 60-80 and TB 60-100, some sulfur-containing signals, like CHS^+ or S^-, show opposite behavior with respect to calcium-containing signals like Ca^+ or $Ca_2PO_3^+$. For example, reduced signal intensities of Ca^+ correspond to enhanced signal intensities of S^- and increased Ca^+-signal intensities correlate with reduced S^--intensities. In contrast, $C_9H_9SO_3^-$, a signal often detected in ToF-SIMS analysis of calciumsulphonate-containing oils, shows a distribution similar to calcium- and phosphorus-containing secondary ions. For the bearing TB 60-100, some local voids in the signal on the raceway can be detected [32].

Two sets of eleven depth profiles, each analyzing positively and negatively charged secondary ions, were carried out on selected spots on the washer surface. In each case, two profiles were recorded outside the raceway (one on the outer and one on the inner side of the washer), and nine profiles were relatively evenly distributed inside the raceway. In order to reduce matrix-induced changes of secondary ion yields and sputtering yields during ion bombardment induced removal of tribological loaded boundary layers and bearing base material, all depth profiles were performed using simultaneous oxygen-flooding applying pure ^{18}O-gas with a base pressure of 1×10^{-6} mbar. As the composition of the tribologically formed boundary layer varies strongly with depth, no reliable information on the actual sputtering yield is known. Therefore, no depth scale was calculated, and the time histories of the intensities of the secondary ion signals are estimated as a function of the measured sputter ion dose densities (SPIDDs) used to remove the boundary layers. As a rough estimation of the depth, it can be determined that with the sputtering parameters used and assuming a constant sputtering yield, applying a SPIDD of 1×10^{16} ion/cm^2 for a pure iron target would have resulted in a crater depth of about 4.5 nm. However, for a multicomponent system built up from highly oxidized layers, as is the case with tribologically formed boundary layers, a significantly reduced and time-dependent sputtering yield must be taken into account. The thickness of the depth-profiled boundary layers was estimated where the curves of the decaying Ca+ signal and the rising Fe+ signal intersect, and the iron substrate is dominant in greater depths. The focus of the ToF-SIMS studies was to gain insight into the temperature effect on the tribofilm formation, so the bearing TB 80-100 was not investigated.

4. Discussion

After the tests, the bearings were inspected to investigate the influence of test conditions on the development of the boundary layers. Besides microscopical investigation, the axial bearing washers were inspected on the raceways by nanoindentational and frictional measurements on circumferential tracks at specific positions. Thus, information on the influence of the bearing rolling elements running conditions regarding pure rolling and rolling with superimposed slip (due to kinematic slip) on the raceways could be obtained. Especially in the hardness measurements for the bearing washers TB 60-120 and TB 60-80 (with long running time in bearing life test), very soft circumference tracks were detected. In the following, the main results of the measurements are compared.

The data for the average frictional torque achieved in the FE8 life tests for the four bearings are depicted in Figure 29. For the bearings with varying temperatures, the frictional torque is, in the case of the bearing TB 60-100, the lowest. Thus, the change of the frictional torque can be referred to as the decrease of the oil's viscosity with increasing temperature. Effects of the tribofilms formed in each case with specific surface properties can play a role. The fourth bearing (TB 80-100) with the increased axial load of 80 kN features the highest average frictional torque.
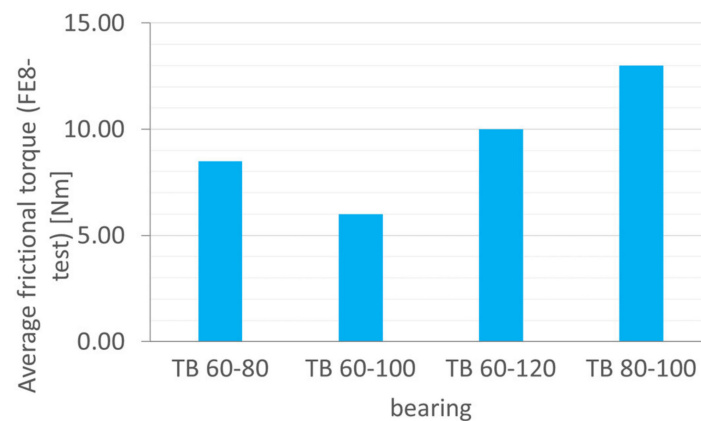

Figure 29. Average frictional torque achieved by FE8 life test for the bearings.

A comparison of the average hardness on the raceways for the tested bearing is shown in Figure 30. The bearings failing in the FE-8 test (TB 60-100 and TB 80-100, tested under 100 °C) feature the highest hardness values within the no-slip zones. Only in the case of the bearing TB 60-80 is the hardness at the no-slip zone lowest. The slip zones were divided into the high slip zone outside (at the Position from 4 to 5 mm) and the high slip zone inside at Positions 10 and 11 mm. The reduced hardness of the bearings passing the test (TB 60-80 and TB 60-120) can be explained by the development of thicker boundary layers resulting in a softer surface.

To prove this behavior, the loading–unloading curves from the nanoindentational tests can be used. Figure 31 depicts a nanoindent on the raceway compared to a nanoindent on an unloaded zone of bearing TB 60-100. For the indent on the unloaded zone, the tip displaces linear with increasing force into the material. In the case of the indent on the raceway, the tip indents much deeper for the same load. The remaining plastic deformation of 50 nm is significantly higher compared to the plastic deformation of 20 nm for the indent in the unloaded zone. The behavior of the indent allows for estimating the thickness of the tribofilm to be at least 30 nm to 40 nm. The boundary layer thickness is in the range of the detected slipping wear scars (compare Figure 12). In this case, the layers have the benefit of protecting the surface against slipping wear.
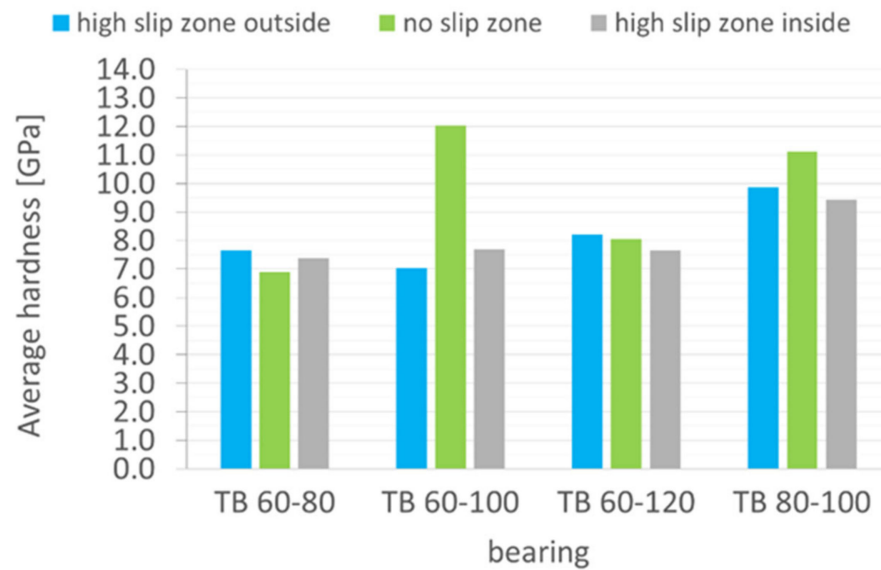
Figure 30. Average hardness on the raceways for the tested bearings.
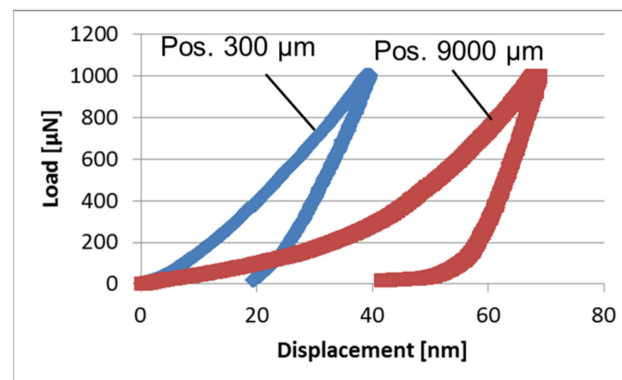

Figure 31. Exemplary indents on bearing TB 60-100 in an unloaded zone (300 μm) and loaded zone (9000 μm).

　　To conclude on the properties of the boundary layers while scratching, the scratch indentation depth at the maximum load of 1 mN during scratch was compared for the no-slip zone and both high slip zones (slip level up to 10%), Figure 32. The indentation depth was calculated by subtraction of the pre-scan profile from the scratch depth at the highest load of the scratch. For the bearings tested under 60 kN load with increasing temperature, the indentation depth decreased in the no-slip and high slip zones. For all bearing washers, the indentation depth on the outer high slip zone is higher than the indentation depth on the no-slip zone. On the inner high slip zones, the indentation depth is the lowest. By increasing the load on the bearing from 60 kN (TB 60-100) to 80 kN (TB 80-100), the indentation depth increased for all zones equally. This can be correlated to the influence of the higher load and increased tangential forces on the surfaces. Due to this, the tribofilm formation is increased, resulting in thicker boundary layers. Previous studies showed the thermal influence on the tribofilm formation is mainly influenced by an increase in the temperature in the range from 20 °C to 70 °C [33]. As the investigations were performed at higher temperatures, the increase in temperature from 80 °C to 100 °C and 120 °C had less influence on the formed tribofilm thickness.
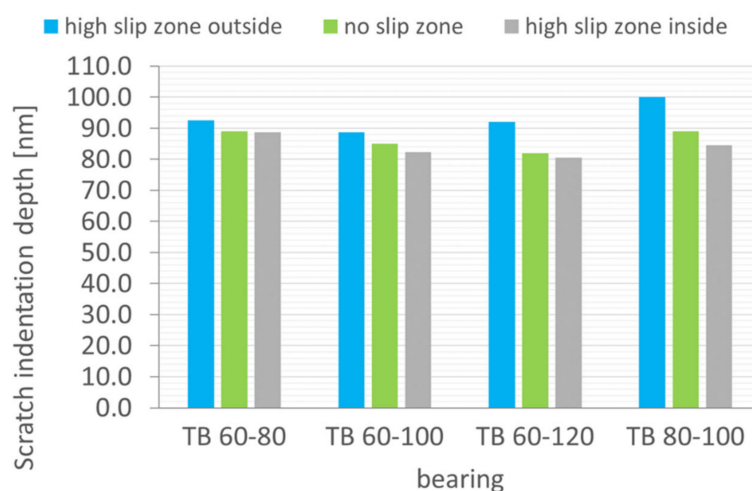
Figure 32. Scratch indentation depth for slip zones of investigated bearing washer.

The average CoF on the raceways for the first test cycle based on the pin-on-disk tribometer is shown in Figure 33. The second (TB 60-100) and third (TB 60-120) bearings feature the highest values. These CoF increased with increasing temperature during the bearing test. Thus, an increased CoF can be referred to as boundary layers with increased frictional properties. The formed tribofilms feature a fine surface roughness with the ability to serve as drainage for the oil in the tribological contact. This effect was observed by Topolovec-Miklozic et al. [34] and can explain the increase in friction, as the oil is easier pushed out of the contact zone. Conversely, the bearing TB 80-100, with the lowest running time in the life test, showed the lowest CoF. In this case, the surface shows the highest hardness values at the zones of high slip (compare Figure 30), and it can be concluded that there is higher compaction due to the higher load and shear forces of the tribofilm.
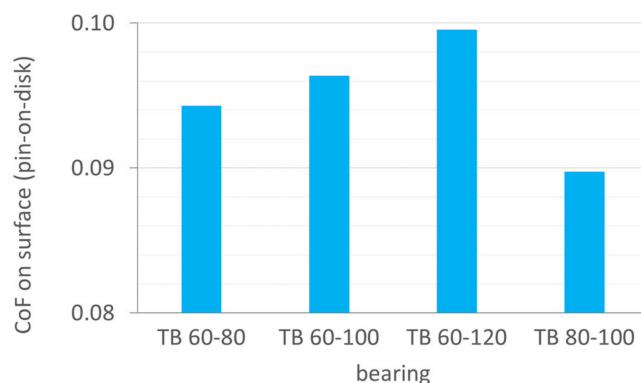

Figure 33. Average CoF (coefficient of friction) measured by pin-on-disk test on the raceways for the tested bearings.

The bearing TB 60-120 showed increased slipping wear on the outer high slip zone. The investigation of the hardness, friction, and film thickness could not prove to be influenced by these factors. Additionally, the tribofilm removal had no negative influence, such as WEC formation. Thus, the susceptibility has to be correlated to the influence of the temperature in combination with high slip to the chemical tribofilm composition. Regarding the ToF-SIMS analysis, we can find on this specific track an increase of the Ca^+, $PO2^-$, and $Ca_2PO_3^-$ signals in comparison to the other positions on the bearing washer. It also has to be remarked that these signals are increased for the whole outer high slip zone and the no-slip zone for the bearing prone to WEC (TB 60-100).

For the different test runs, Figure 34 shows a comparison of the Ca^+-signal intensity distribution according to ToF-SIMS-large area map analysis, the results of hardness mea-

surements on selected positions (dashed line), and the SPIDDs (sputter ion dose densities) needed to reach the Ca^+-/Fe^+-crossing point (solid line) as a function of the distance from the outer rim. As can be seen from the solid lines, different values of SPIDDs are needed on different spots of the raceway of each test bearing to remove the boundary layer indicating different layer thicknesses.
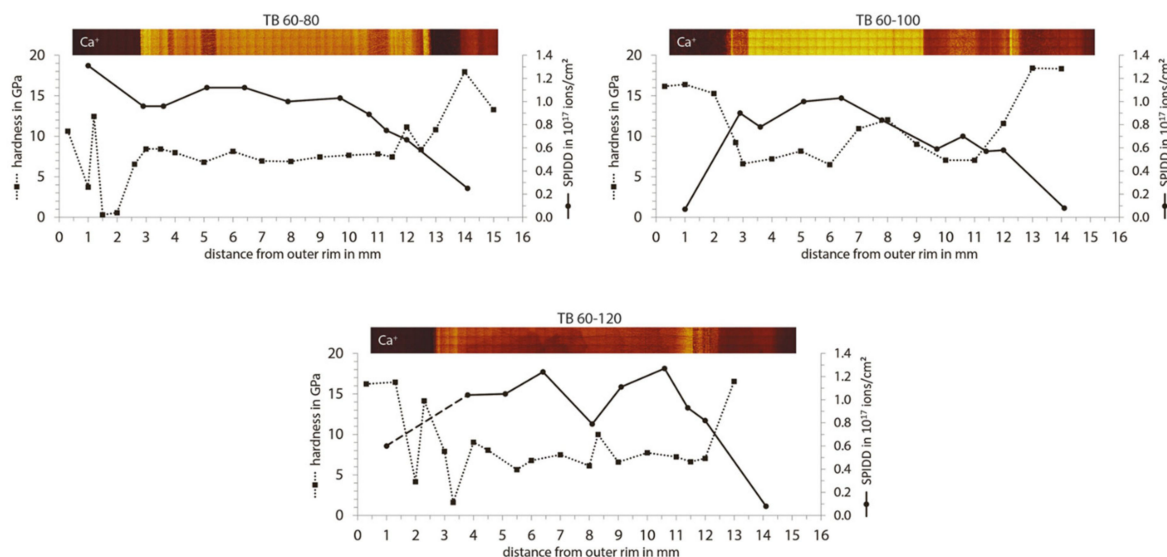

Figure 34. Large area map of Ca^+, hardness values (dashed line), and SPIDDs needed to reach the Ca^+-/Fe^+-crossing point (solid line) as a function of distance from outer rim obtained from test bearings TB 60-80 and TB 60-100 (top) and TB 60-120 (bottom). (Note, due to problems while analyzing TB 60-120, the second data point of the SPIDD-curve is missing, indicated by a dashed part of the solid line.).

Different thicknesses of the boundary layers in the regions presented are confirmed by the results of hardness measurements (Figure 30), taking into account that reduced values of hardness from nanoindentation can be explained by different layer thicknesses of non-metallic layers. Note that the hardness values were measured on the opposite washer assuming equal behavior compared to the washer analyzed with ToF-SIMS, which was verified with TB 60-100, where both washers were characterized by nanoindentation. Nevertheless, minor discrepancies cannot be ruled out.

From the diagrams in Figure 34, it can be seen that the measured hardness values within the raceway (approx. 2.7–12.7 mm from the outer rim) are mostly in the range of 6 to 8 GPa. As can be seen as well, in most of the areas of reduced hardness within the raceways, SPIDDs of at least $1 \cdot 10^{17}$ ions/cm^2 are needed to reach the Ca^+-/Fe^+-crossing point. On the other side, areas where hardness values exceed approx. 8 GPa correlate with regions where corresponding SPIDDs of less than $1 \cdot 10^{17}$ ions/cm^2 indicate reduced boundary layer thicknesses or layer densities. Nevertheless, with respect to those SPIDDs applied during depth profiles inside the raceway, some differences but also similarities become visible comparing bearing TB 60-120 with the other ones.

On the one hand, considering the course of SPIDD-values needed to reach the Ca^+-/Fe^+-crossing point at spots inside the raceway (see Figure 35), all bearings show a slight increase within a distance of approx. 5 mm from the outer rim. In contrast to TB 60-120, where the SPIDD-values remain the same to a large extent up to a distance of approx. 10 mm before decreasing, both TB 60-100 and TB 60-80 already show an onset of decreasing SPIDD-values at a distance of about 7 mm from the outer rim, which is close to the no-slip zone. Although comparable in the point of onset, the SPIDD-values of TB 60-100 show a much steeper decrease compared to those of TB 60-80.
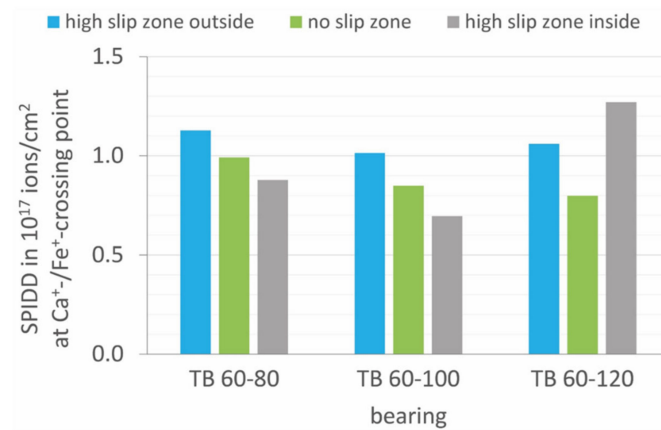
Figure 35. SPIDDs needed to reach the Ca^+-/Fe^+-crossing point (solid line) obtained from test bearings TB 60-80, TB 60-100, and TB 60-120.

On the other hand, comparing SPIDD-values needed to reach the Ca^+-/Fe^+-crossing point in an area at the outside edge (approx. 2.7–5.0 mm from the outer rim) and the inside edge (approx. 10.0–12.7 mm) of the raceway one can see that with all bearings lower SPIDD-values were determined at the inside edge of the raceway. One reason for this could possibly be different amounts of the specific friction energy accumulated at the outer or inner edge of the raceway of this cylindrical roller bearing, as proposed in [35].

In the case of the bearing TB 60-100, the formed tribofilm is on the high slip zones thinner than for bearing TB 60-80 and bearing TB 60-120. In the case of the ToF-SIMS large area mappings (Figure 28), on the surface, the highest intensity for the Ca^+ signal could be detected. This can cause in combination with the formation of a Ca^+ and CaO^- enriched tribofilm hydrogen formation and easier diffusion, see Figure 36. In this case, the hydrogen can diffuse to the steel subsurface while the oxygen combines with calcium.
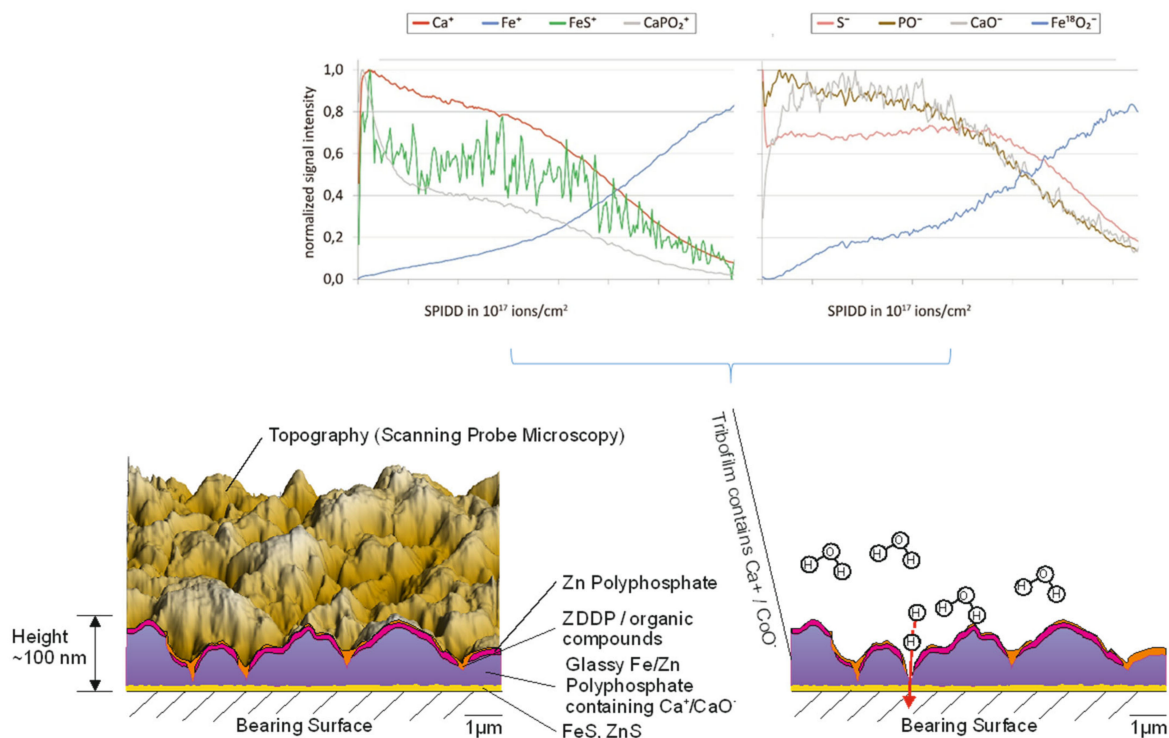

Figure 36. Hydrogen diffusion through voids on Ca^+/CaO^- rich tribofilm.

5. Conclusions

A micro-tribological investigation of the bearings' surfaces after life tests provides relevant knowledge about boundary layers. The measured data can be correlated to the bearings' lifetimes. The data show that the measured CoF in the micro pin-on-disk tester cannot be directly compared to the torque measurements gained in the FE8 life test. This can be attributed to the different kinematics as well as the dry contact in the micro pin-on-disk tester compared to the lubricated contact in the bearing test rig. The axial bearing washers tested under 100 °C with the low additivated oil generally result in early failure and white etching cracks under the surface. By a change of the applied temperature for the tests, the bearing life can be increased significantly. The temperature has the main influence on the formed tribofilms and WEC formation. Having a detailed look at the bearing washers, the influence of the slip in comparison to pure rolling is obvious.

For the bearings with longer lifetimes, different properties of the boundary layers can be detected. The tests allow concluding the formation of advantageous boundary layers.

- It could be proven by nano scratch tests that the decreased hardness cannot only be measured under the contact of the tip used for the nanoindents. The soft layers are distributed for a larger field and result in wider scratches on the surface. To improve the bearing life, these boundary layers should provide soft properties combined with a higher CoF compared to boundary layers on bearings with earlier failure.
- This can be proven as well in micro pin-on-disk tests. The early failed bearings feature a lower CoF on the surface between 0.9 and 1, while the bearing washers run at 80 °C and 120 °C feature higher frictional properties on the surface. Thus, a change in the running conditions changes the tribochemical reactions on the surface and results in preferable boundary layers.
- It could also be shown that slipping wear with partial tribofilm loss does not result in subsurface WEC formation.
- To investigate differences in the chemical composition of the boundary layers, ToF-SIMS (Time-of-Flight Secondary Ion Mass Spectrometry) was performed on the bearing surfaces. For the bearing running at 120 °C, large area mappings show a more or less uniform distribution of secondary ion signals inside the rolling contact area. In contrast, with both bearings run at lower temperatures, several secondary ion signals show inhomogeneous distributions inside the raceway much more pronounced for the bearing, where a tendency for white etching cracks was observed. ToF-SIMS-depth profiles show non-uniform values for boundary layer thicknesses across the rolling contact areas of the bearing washers tested at 60 kN with some correlations with respect to local values of hardness from nanoindentation. The reduced values of hardness can be explained by increased layer thicknesses of non-metallic layers. The thickness of these layers is estimated to be a few 10 nm. The intensity of Ca^+ signals for the bearing TB 60-100 (failed due to WEC) is increased. On the outer high slip zone, the SPIDD-values needed to reach the Ca^+-/Fe^+-crossing is highest, which is also the zone of subsurface WEC found by ultrasonic studies (Figure 3b). It has to be remarked that calcium, in combination with water molecules, promotes hydrogen formation; this effect can be assisted by the increase in temperature in the tribological contact. Thus, the higher calcium amount can lead to increased WEC formation.

In case of slippage wear, the boundary layers seem to protect the original surface. It could be proven that not only the mechanical properties of the boundary layers are influenced by the test conditions. In addition, an influence on the friction coefficient was observed. For additional future investigations, attention should be paid to the void surface signals for the failed bearing TB 60-100 and the content of Ca^+ and CaO^- in the film. Maybe a cause can be found for easier subsurface WEC formation and hydrogen diffusive processes.

Conflicts of Interest: The authors declare no conflict of interest. The funders had no role in the design of the study; in the collection, analyses, or interpretation of data; in the writing of the manuscript, or in the decision to publish the results.

References

1. Gould, B.; Greco, A. Investigating the Process of White Etching Crack Initiation in Bearing Steel. *Tribol. Lett.* **2016**, *62*, 26. [CrossRef]
2. Gould, B.; Greco, A.; Stadler, K.; Xiao, X. An analysis of premature cracking associated with microstructural alterations in an AISI 52100 failed wind turbine bearing using X-ray tomography. *Mater. Des.* **2017**, *117*, 417–429. [CrossRef]
3. Ooi, S.; Gola, A.; Vegter, R.H.; Yan, P.; Stadler, K. Evolution of white-etching cracks and associated microstructural alterations during bearing tests. *Mater. Sci. Technol.* **2017**, *33*, 1657–1666. [CrossRef]
4. Evans, M.-H. An updated review: White etching cracks (WECs) and axial cracks in wind turbine gearbox bearings. *Mater. Sci. Technol.* **2016**, *32*, 1133–1169. [CrossRef]
5. Phorer, B. Analyse des Zusammenhangs zwischen dem tribochemischen Aufbau von Grenzschichten und der Ausbildung von White Etching Crack Schäden. Ph.D. Thesis, Friedrich-Alexander-Universität Erlangen-Nürnberg, Nürnberg, Germany, 2022.
6. Ruellan, A.; Kleber, X.; Ville, F.; Cavoret, J.; Liatard, B. Understanding white etching cracks in rolling element bearings: Formation mechanisms and influent tribochemical drivers. *Proc. Inst. Mech. Eng. Part J J. Eng. Tribol.* **2015**, *229*, 886–901. [CrossRef]
7. Zhang, J.; Spikes, H. On the Mechanism of ZDDP Antiwear Film Formation. *Tribol. Lett.* **2016**, *63*, 24. [CrossRef]
8. Tripaldi, G.; Vettor, A.; Spikes, H. Friction Behaviour of ZDDP Films in the Mixed, Boundary/EHD Regime. *SAE Trans.* **1996**, *105*, 1819–1830. [CrossRef]
9. Gosvami, N.N.; Bares, J.A.; Mangolini, F.; Konicek, A.R.; Yablon, D.G.; Carpick, R.W. Mechanisms of antiwear tribofilm growth revealed in situ by single-asperity sliding contacts. *Science* **2015**, *348*, 102–106. [CrossRef]
10. Benedet, J.; Green, J.H.; Lamb, G.D.; Spikes, H.A. Spurious Mild Wear Measurement Using White Light Interference Microscopy in the Presence of Antiwear Films. *Tribol. Trans.* **2009**, *52*, 841–846. [CrossRef]
11. Fujita, H.; Spikes, H.A. The formation of zinc dithiophosphate antiwear films. *Proc. Inst. Mech. Eng. Part J J. Eng. Tribol.* **2004**, *218*, 265–278. [CrossRef]
12. Mosey, N.; Woo, T.; Kasrai, M.; Norton, P.; Bancroft, G.; Müser, M. Interpretation of experiments on ZDDP anti-wear films through pressure-induced cross-linking. *Tribol. Lett.* **2006**, *24*, 105–114. [CrossRef]
13. Dorgham, A.; Azam, A.; Morina, A.; Neville, A. On the Transient Decomposition and Reaction Kinetics of Zinc Dialkyldithiophosphate. *ACS Appl. Mater. Interfaces* **2018**, *10*, 44803–44814. [CrossRef] [PubMed]
14. Sharma, V.; Erdemir, A.; Aswath, P. An analytical study of tribofilms generated by the interaction of ashless antiwear additives with ZDDP using XANES and nano-indentation. *Tribol. Int.* **2015**, *82*, 43–57. [CrossRef]
15. Tang, H.; Wang, L.-P.; Gui, J.; Kuo, D. Experimental and analytical studies of dynamic friction at the head/disk interface. *Tribol. Int.* **2000**, *33*, 343–351. [CrossRef]
16. Bhushan, B. Adhesion and stiction: Mechanisms, measurement techniques, and methods for reduction. *J. Vac. Sci. Technol. B Microelectron. Nanometer Struct. Process. Meas. Phenom.* **2003**, *21*, 2262–2296. [CrossRef]
17. Fu, T.C.; Suzuki, S. Low stiction/low glide height head–disk interface for high-performance disk drives. *J. Appl. Phys.* **1999**, *85*, 5600–5605. [CrossRef]
18. Tohyama, M.; Ohmori, T.; Murase, A.; Masuko, M. Friction reducing effect of multiply adsorptive organic polymer. *Tribol. Int.* **2009**, *42*, 926–933. [CrossRef]
19. Wiendl, S.; Zabel, W.-R.; Poll, G.; Gatzen, H.-H. The Influence of boundary layer properties on grease lubricated high-speed ball bearing performance. *Tribol. Ser.* **2003**, *43*, 441–447. [CrossRef]
20. Gatzen, M.; Pape, F.; Bruening, C.; Gatzen, H.; Arlinghaus, H.; Poll, G. Correlation between performance and boundary layers in high speed bearings lubricated with polymer-enhanced greases. *Tribol. Int.* **2010**, *43*, 981–989. [CrossRef]

21. Oliver, W.C.; Pharr, G.M. An improved technique for determining hardness and elastic modulus using load and displacement sensing indentation experiments. *J. Mater. Res.* **1992**, *7*, 1564–1583. [CrossRef]

22. Pape, F. Mikrotribologische Untersuchungen an Wälzlagern mit polymeradditivierter Fettschmierung (Microtribological Investigations of Roller Bearings Lubricated with Greases Containing Polymer Additives). Ph.D. Thesis, Leibniz University Hanover, Hanover, Germany, 2011.

23. Pape, F.; Rissing, L.; Gatzen, H.H. Fabrication and Tribological Investigation of Fullerene C60/C70 Reinforced Epoxy Resin SU-8. *Tribol. Und Schmier.* **2011**, *58*, 51–55.

24. Benninghoven, A.; Rudenauer, F.G.; Werner, H.W. *Secondary Ion Mass Spectrometry: Basic Concepts, Instrumental Aspects, Applications and Trends*; Chemical Analysis; Wiley: New York, NY, USA, 1987; Volume 86.

25. Vickerman, J.C.; Briggs, D. (Eds.) *ToF-SIMS: Materials Analysis by Mass Spectrometry*, 2nd ed.; IM Publications: Chichester, UK, 2013.

26. Arlinghaus, H.F. Static Secondary Ion Mass Spectrometry. In *Surface and Thin Film Analysis*, 2nd ed.; Bubert, H., Jenett, H., Eds.; Wiley-VCH: Weinheim, Germany, 2011.

27. Minfray, C.; Martin, J.M.; De Barros, M.I.; Mogne, T.L.; Kersting, R.; Hagenhoff, B. Chemistry of ZDDP tribofilm by ToF-SIMS. *Tribol. Lett.* **2004**, *17*, 351–357. [CrossRef]

28. Kubo, T.; Fujiwara, S.; Nanao, H.; Minami, I.; Mori, S. TOF-SIMS analysis of boundary films derived from calcium sulfonates. *Tribol. Lett.* **2006**, *23*, 171–176. [CrossRef]

29. Murase, A.; Mori, H.; Ohmori, T. TOF-SIMS analysis of friction surfaces of hard coatings tested in engine oil. *Appl. Surf. Sci.* **2008**, *255*, 1494–1497. [CrossRef]

30. Lipinsky, D.; Brüning, C.; Mayer, C.; Arlinghaus, H.F.; Skubacz, T.; Poll, G. Oberflächenanalyse der aus Additiven gebildeten tribologischen Schichten mit der Flugzeit-Sekundärionenmassenspektrometrie. *Tribol. Schmier.* **2011**, *58*, 29–35.

31. Mayer, C.; Lipinsky, D.; Wohlleber, F.; Pflaum, H.; Stahl, K.; Arlinghaus, H.F. Coordinated test-rig and ToF-SIMS experiments to investigate the influence of phosphate glass layers on the friction behavior of a wet clutch. *Surf. Interface Anal.* **2014**, *46*, 401–404. [CrossRef]

32. Muhmann, C. Untersuchung der unter tribologischer Belastung auf Laufflächen von Axial-Zylinderrollenlagern gebildeten Grenzschichten mittels ToF-SIMS und Nanoindentation. Ph.D. Thesis, Westfälische Wilhelms-Universität Münster, Münster, Germany, 2018.

33. Pape, F.; Poll, G.; Mallach, D.; Lipinsky, D.; Arlinghaus, H.F.; Matthias, T.; Behrens, B.A. Investigations of ZDDP tribofilm formation regarding temperature influences. In Proceedings of the Bearing World Conference, Online, 19–23 October 2020.

34. Topolovec-Miklozic, K.; Forbus, T.R.; Spikes, H.A. Film thickness and roughness of ZDDP antiwear films. *Tribol. Lett.* **2007**, *26*, 161–171. [CrossRef]

35. Loos, J.; Kruhoeffer, W. Einfluss der Reibbeanspruchung auf die WEC-Bildung in Wälzlagern. *Tribol. Schmier.* **2014**, *62*, 33–43.